IET Control Theory & Applications

Research Article

IET Journals
The Institution of Engineering and Technology

Saturated adaptive sliding mode control for autonomous vessel landing of a quadrotor

ISSN 1751-8644
Received on 17th September 2017
Revised 18th January 2018
Accepted on 16th April 2018
E-First on 16th May 2018
doi: 10.1049/iet-cta.2017.0998
www.ietdl.org

Yanting Huang[1,2], Zewei Zheng[1], Liang Sun[3] ✉, Ming Zhu[2]

[1]*The Seventh Research Division, School of Automation Science and Electrical Engineering, Beihang University, Beijing 100191, People's Republic of China*

[2]*School of Aeronautic Science and Engineering, Beihang University, Beijing 100191, People's Republic of China*

[3]*School of Automation and Electrical Engineering, University of Science and Technology Beijing, Beijing 100083, People's Republic of China*

✉ *E-mail: liangsun@ustb.edu.cn*

Abstract: An autonomous vessel landing control algorithm of a quadrotor with input saturation and parametric uncertainties is investigated. To facilitate the controller design, the problem of vessel landing is converted from general trajectory tracking problem of a quadrotor to a stabilisation problem of relative motion. A non-linear and coupled six-degrees-of-freedom relative position and attitude model with uncertain parameters and external disturbances is established. The proposed controllers are composed of a relative position controller (RPC) and a relative attitude-altitude controller (RAC). The quadrotor is first commanded by RPC to reach above the vessel, as it reaches, RAC is initiated to guide the quadrotor to descend steadily on the vessel. Both RPC and RAC employ the saturated adaptive sliding mode control technique. The parametric uncertainties and disturbances are estimated by adaptive algorithms, while the control input saturation effect is compensated by linear compensators. All signals in the closed-loop systems are proved uniformly ultimately bounded via Lyapunov theory. Numerical simulations validate the effectiveness of the proposed control approach.

1 Introduction

With the development of the quadrotor helicopter, considerable researches focused on its design, analysis, and operations have been performed. Compared with the conventional helicopters, quadrotors have many advantages including versatile manoeuvrability, hovering capacity, and simple mechanical structure [1, 2]. Therefore, They are used in several typical missions, such as search and rescue missions, surveillance, inspection, aerial cinematography [3]. In particular, when there is a need for performing hidden missions, quadrotors are the best choice on account of theirs advantages of small size and excellent operation capabilities. Additionally, the application of quadrotors in open seas can provide the capability of efficient reconnaissance and survey on the ocean. However, it is necessary to equip with a vessel as corresponding mobile platform for a quadrotor, since the quadrotor has a limitation in time of endurance. In this case, autonomous landing task on the vessel is crucial for the quadrotor. Meanwhile, it is also challenging to perform autonomous vessel landing because of pseudorandom vessel motion caused by tanglesome wave interaction [4]. Besides, the time-varying disturbances from the airflow and the ocean currents are unpredictable [5]. All of these make the vessel landing control problem particularly complicated.

A variety of methods have been proposed to solve autonomous landing problem. In [5], the authors introduced an algorithm composed of the time-delay controller and the guidance law for shipboard landing considering model uncertainties and unpredictable disturbances. An adaptive sliding mode control for landing fixed-wing unmanned aerial vehicles on carrier was presented in [6]. Moreover, coordinated landing control was designed in [7] so that unmanned aerial vehicle can track the generalised landing trajectory generated by the optimisation of the steady landing condition. Optimisation approach has been utilised in automatic carrier landing system [8] as well, the authors presented a novel method based on simplified brain storm optimisation algorithm to optimise the control parameters. Other landing methods include vision-guided landing methods [9, 10], parameters optimisation algorithm [11, 12], and invariant ellipsoid method [4].

Nevertheless, aforementioned landing methods mainly pay attention to the control design of aircraft aiming at controlling the aircraft to track the motion trajectory of the landing platform. Besides, most platforms are two-degrees-of-freedom (2-DOF) platforms [10] or a simple moving platform [11], which have a certain gap with the practical application. In this case, we introduce the relative motion modelling method [13] to establish the relative model of the quadrotor and vessel. The relative modelling method can convert the vessel landing problem from general trajectory tracking problem of a quadrotor to a stabilisation problem of relative motion, which is enlightened by the application of the relative model in spacecraft rendezvous system [14, 15]. As for the vessel model, it is feasible to establish vessel model by using sinusoidal functions in [16] or physical model in [17]. To take the ship physical model into account and aviod complexity, we use a simple physical model that consists of sinusoidal functions [18] and 3-DOF physical model [19] in this paper.

Input saturation effect should be considered in vessel landing controller design. Due to the inevitability of input saturation in practical systems, the system performance may be severely degenerated and the closed-loop system even be instable [20]. To handle the input saturation, many research attempts have been carried out. Considering the non-differentiable asymmetric input saturation in the trajectory tracking control of surface vessel, Zheng *et al.* [21] employed a smooth hyperbolic tangent function to approximate the saturation function and introduced a Nussbaum function to compensate the saturation approximation. Based on the nested saturation method, inner-outer loop control for quadrotor was presented in [22]. Stable anti-windup compensator and disturbance observer were employed to handle the effect of input saturation in spacecraft attitude control systems [23, 24] and surface vessel systems [25, 26]. Specifically, the anti-windup re-configurable sliding mode control strategy presented in [27, 28] ensures the close-loop system finite-time stability without violation of actuator limits. However, the landing researches considering input saturation are quite limited.

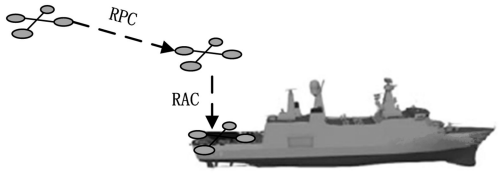

Fig. 1 *Process of automatic landing*

In this paper, we mainly present an automatic vessel landing control algorithm for a quadrotor using relative motion model with uncertain parameters, input saturation, and external disturbances. On account of under-actuated property of the relative motion model, the whole autonomous landing operation proceeds in two phases: the approaching phase and the descent phase (see in Fig. 1) [16]. In the first stage, the quadrotor is approached to hover above the vessel by relative position controller (RPC). In the second stage, the quadrotor selects appropriate time to descend vertically to the vessel by relative attitude–altitude controller (RAC). The main contributions of this paper are summarised as follows. (i) Compared with our previous work [29] where the novel relative dynamics between quadrotor and ship are modelled but external disturbances and model uncertainty are ignored, a 6-DOF non-linear relative motion model with uncertainty and aerodynamic disturbances model is established. (ii) Compared with autonomous landing of a quadrotor on a 2-DOF moving platform in [30] and autonomous landing on a 3-DOF moving ship in [29], 6-DOF vessel motion is considered to show the practical motion more comprehensively. (iii) Compared with landing method [10, 11, 16, 30] without consideration of model uncertainty and input saturation, adaptive sliding mode method is employed in both RPC and RAC to deal with model uncertainty, and anti-windup compensator is utilised to tackle the problem of input saturation. Specially, inner-outer loop design and the second-order command filter are utilised in RPC to handle strong coupled property of the relative model. (v) The landing position errors are addressed by Monte-Carlo simulation to verify the robustness of the proposed controller to random external perturbation.

The layout of the paper is arranged as follows. Some preliminaries are presented in Section 2. The 6-DOF relative model and objective are stated in Section 3. It is devoted to design RPC and RAC in Section 4. In Section 5, numerical simulations are performed to verify the proposed approach, followed by conclusion in Section 6.

2 Preliminaries

Throughout this paper, the following notations are adopted. $|\cdot|$ denotes the absolute value of a scalar or the absolute value of each components for a vector, i.e. for a vector $\boldsymbol{x} = [x_1, x_2, \ldots, x_n]^{\mathrm{T}} \in \mathbb{R}^n$, $|\boldsymbol{x}| = [|x_1|, |x_2|, \ldots, |x_n|]^{\mathrm{T}}$. $\|\cdot\|$ denotes the Euclidean norm of a vector or the Frobenius norm of a matrix. $\lambda_{\max}(\boldsymbol{A})$ denotes the biggest eigenvalue of a square matrix $\boldsymbol{A}$. For any vector $\boldsymbol{x} \in \mathbb{R}$, the saturation function is defined as

$$\mathrm{sat}(x) = \begin{cases} x_{\max}, & x > x_{\max} \\ x, & x_{\min} \le x \le x_{\max} \\ x_{\min}, & x < x_{\min} \end{cases}$$

where $x_{\min}$ and $x_{\max}$ are the lower and upper bounds of saturation constraints. For any vector $\boldsymbol{x} = [x_1, x_2, \ldots, x_n]^{\mathrm{T}} \in \mathbb{R}^n$, the saturation function vector is

$$\mathrm{Sat}(x) = [\mathrm{sat}(x_1), \mathrm{sat}(x_2), \ldots, \mathrm{sat}(x_n)]^{\mathrm{T}}.$$

3 Problem formulation

3.1 Reference frames

The related frames are illustrated in Fig. 2, the inertial frame and body-fixed frames of the quadrotor and the vessel are defined, respectively. The inertial frame $\mathcal{F}_e = \{O_e, \boldsymbol{x}_e, \boldsymbol{y}_e, \boldsymbol{z}_e\}$ is fixed on the

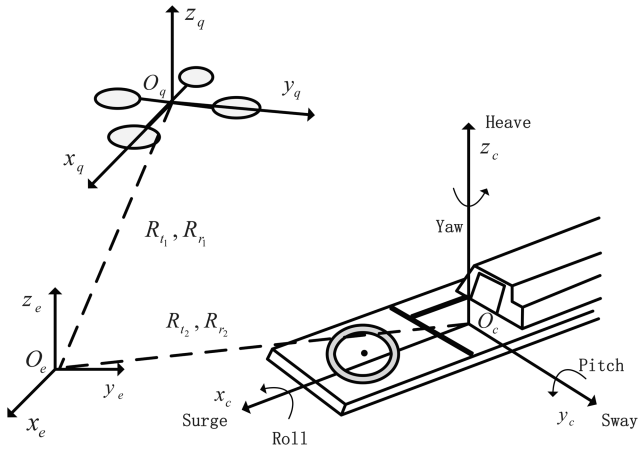

Fig. 2 *Reference frames*

earth. The frames $\mathcal{F}_q = \{O_q, \boldsymbol{x}_q, \boldsymbol{y}_q, \boldsymbol{z}_q\}$ and $\mathcal{F}_c = \{O_c, \boldsymbol{x}_c, \boldsymbol{y}_c, \boldsymbol{z}_c\}$ represent the body frames of the quadrotor and the vessel, respectively. O_q and O_c are the geometric centre points of the quadrotor and the vessel, respectively.

3.2 Models of the quadrotor and the vessel

According to [31], the kinematic equations of the quadrotor can be expressed as

$$\begin{cases} \dot{\boldsymbol{\xi}}_1 = \boldsymbol{R}_{t_1} \boldsymbol{V}_1 \\ \dot{\boldsymbol{\eta}}_1 = \boldsymbol{R}_{r_1} \boldsymbol{\Omega}_1 \end{cases} \tag{1}$$

where $\boldsymbol{\xi}_1 = [x_1, y_1, z_1]^{\mathrm{T}}$ and $\boldsymbol{\eta}_1 = [\phi_1, \theta_1, \psi_1]^{\mathrm{T}}$ (consists of the roll angle ϕ_1, pitch angle θ_1, and yaw angle ψ_1) denote the position vector and attitude vector of quadrotor in the frame $\mathcal{F}_e$, respectively. $\boldsymbol{V}_1 = [u_1, v_1, w_1]^{\mathrm{T}}$ and $\boldsymbol{\Omega}_1 = [p_1, q_1, r_1]^{\mathrm{T}}$ are the velocity vector and angular velocity vector in the frame $\mathcal{F}_q$, respectively. The rotation matrix $\boldsymbol{R}_{t_1}$ and transformation matrix $\boldsymbol{R}_{r_1}$ are given by

$$\boldsymbol{R}_{t_1} = \begin{bmatrix} \mathrm{c}_{\theta_1}\mathrm{c}_{\psi_1} & \mathrm{s}_{\theta_1}\mathrm{c}_{\psi_1}\mathrm{s}_{\phi_1} - \mathrm{s}_{\psi_1}\mathrm{c}_{\phi_1} & \mathrm{s}_{\theta_1}\mathrm{c}_{\psi_1}\mathrm{c}_{\phi_1} + \mathrm{s}_{\psi_1}\mathrm{s}_{\phi_1} \\ \mathrm{c}_{\theta_1}\mathrm{s}_{\psi_1} & \mathrm{s}_{\theta_1}\mathrm{s}_{\psi_1}\mathrm{s}_{\phi_1} + \mathrm{c}_{\psi_1}\mathrm{c}_{\phi_1} & \mathrm{s}_{\theta_1}\mathrm{s}_{\psi_1}\mathrm{c}_{\phi_1} - \mathrm{c}_{\psi_1}\mathrm{s}_{\phi_1} \\ -\mathrm{s}_{\theta_1} & \mathrm{c}_{\theta_1}\mathrm{s}_{\phi_1} & \mathrm{c}_{\theta_1}\mathrm{c}_{\phi_1} \end{bmatrix}$$

$$\boldsymbol{R}_{r_1} = \frac{1}{\mathrm{c}_{\theta_1}} \begin{bmatrix} \mathrm{c}_{\theta_1} & \mathrm{s}_{\phi_1}\mathrm{s}_{\theta_1} & \mathrm{c}_{\phi_1}\mathrm{s}_{\theta_1} \\ 0 & \mathrm{c}_{\phi_1}\mathrm{c}_{\theta_1} & -\mathrm{s}_{\phi_1}\mathrm{c}_{\theta_1} \\ 0 & \mathrm{s}_{\phi_1} & \mathrm{c}_{\phi_1} \end{bmatrix}$$

where $\mathrm{s}_{(\cdot)} \triangleq \sin(\cdot)$, $\mathrm{c}_{(\cdot)} \triangleq \cos(\cdot)$. In addition, we have $\dot{\boldsymbol{R}}_{t_1} = \boldsymbol{R}_{t_1} \boldsymbol{S}(\boldsymbol{\Omega}_1)$, where $\boldsymbol{S}(\boldsymbol{\Omega}_1)$ is the skew-symmetric matrix defined as

$$\boldsymbol{S}(\boldsymbol{\Omega}_1) = \begin{bmatrix} 0 & -r_1 & q_1 \\ r_1 & 0 & -p_1 \\ -q_1 & p_1 & 0 \end{bmatrix}$$

The dynamics of quadrotor can be expressed by [31]

$$\begin{cases} m_1 \dot{\boldsymbol{V}}_1 + m_1 \boldsymbol{S}(\boldsymbol{\Omega}_1) \boldsymbol{V}_1 = \boldsymbol{F} - \boldsymbol{F}_{\mathrm{aero}} - \boldsymbol{F}_{\mathrm{grav}} + \boldsymbol{d}_f \\ \boldsymbol{I}_1 \dot{\boldsymbol{\Omega}}_1 + \boldsymbol{S}(\boldsymbol{\Omega}_1) \boldsymbol{I}_1 \boldsymbol{\Omega}_1 = \boldsymbol{\tau} - \boldsymbol{T}_{\mathrm{aero}} + \boldsymbol{d}_m \end{cases} \tag{2}$$

where m_1 denotes the mass of the quadrotor, $\boldsymbol{I}_1 = \mathrm{diag}\{I_x, I_y, I_z\}$ is the total inertial matrix of the quadrotor. $\boldsymbol{F} = [0, 0, F_{\mathrm{total}}]^{\mathrm{T}}$ and $\boldsymbol{\tau} = [\tau_x, \tau_y, \tau_z]^{\mathrm{T}}$ are, respectively, propeller thrust and torque of the quadrotor, with $F_{\mathrm{total}} = \sum_{i=1}^{4} F_i$, $M_x = d(F_2 - F_4)$, $M_y = d(F_3 - F_1)$, $M_z = c\sum_{i=1}^{4}(-1)^{i+1} F_i$. The forces $F_i (i = 1, 2, 3, 4)$ are the

thrusts generated by the multi-propellers, $d \in \mathbb{R}$ is the distance from the rotor axes to the epicentre of the quadrotor and $c > 0$ is the drag factor. $\boldsymbol{F}_{\text{aero}}$, $\boldsymbol{F}_{\text{grav}}$, and $\boldsymbol{T}_{\text{aero}}$ are aerodynamic force, gravity, and aerodynamic torques, which are described as $\boldsymbol{F}_{\text{aero}} = \boldsymbol{K}_t \boldsymbol{V}_1$, $\boldsymbol{F}_{\text{grav}} = m_1 \boldsymbol{R}_{t_1}^{\mathrm{T}} \boldsymbol{g}$, $\boldsymbol{T}_{\text{aero}} = \boldsymbol{K}_r \boldsymbol{\Omega}_1$, respectively, where $\boldsymbol{K}_t = \text{diag}\{k_{t_1}, k_{t_2}, k_{t_3}\}$ and $\boldsymbol{K}_r = \text{diag}\{k_{r_1}, k_{r_2}, k_{r_3}\}$ are aerodynamic friction matrices, $\boldsymbol{g} = [0, 0, g_s]^{\mathrm{T}} (g_s = 9.8\,\text{m/s})$ is the gravity vector. $\boldsymbol{d}_f$ and $\boldsymbol{d}_m$ include the aerodynamic disturbances such as turbulence and gusts modelled in the simulations section.

From (1) and (2), the second-order derivative of $\boldsymbol{\xi}_1$ with respect to time gives

$$\ddot{\boldsymbol{\xi}}_1 = \frac{h(\boldsymbol{\eta}_1) F_{\text{total}} - \boldsymbol{K}_t \boldsymbol{R}_{t_1} \boldsymbol{V}_1 + \boldsymbol{R}_{t_1} \boldsymbol{d}_f}{m_1} - \boldsymbol{g} \tag{3}$$

where $h(\boldsymbol{\eta}_1)$ is the last column of $\boldsymbol{R}_{t_1}$.

Similar with the kinematics of quadrotor, the kinematics of vessel can be expressed as [32]

$$\begin{cases} \dot{\boldsymbol{\xi}}_2 = \boldsymbol{R}_{t_2} \boldsymbol{V}_2 \\ \dot{\boldsymbol{\eta}}_2 = \boldsymbol{R}_{r_2} \boldsymbol{\Omega}_2 \end{cases} \tag{4}$$

where $\boldsymbol{\xi}_2 = [x_2, y_2, z_2]^{\mathrm{T}}$ and $\boldsymbol{\eta}_2 = [\phi_2, \theta_2, \psi_2]^{\mathrm{T}}$ are the position vector and attitude vector of the vessel in the frame $\mathcal{F}_e$, respectively. $\boldsymbol{V}_2 = [u_2, v_2, w_2]^{\mathrm{T}}$ and $\boldsymbol{\Omega}_2 = [p_2, q_2, r_2]^{\mathrm{T}}$ are the velocity and the angular velocity of the vessel defined in the frame $\mathcal{F}_c$, respectively. $\boldsymbol{R}_{t_2}$ and $\boldsymbol{R}_{r_2}$ are given by

$$\boldsymbol{R}_{t_2} = \begin{bmatrix} \mathrm{c}_{\theta_2}\mathrm{c}_{\psi_2} & \mathrm{s}_{\theta_2}\mathrm{c}_{\psi_2}\mathrm{s}_{\phi_2} - \mathrm{s}_{\psi_2}\mathrm{c}_{\phi_2} & \mathrm{s}_{\theta_2}\mathrm{c}_{\psi_2}\mathrm{c}_{\phi_2} + \mathrm{s}_{\psi_2}\mathrm{s}_{\phi_2} \\ \mathrm{c}_{\theta_2}\mathrm{s}_{\psi_2} & \mathrm{s}_{\theta_2}\mathrm{s}_{\psi_2}\mathrm{s}_{\phi_2} + \mathrm{c}_{\psi_2}\mathrm{c}_{\phi_2} & \mathrm{s}_{\theta_2}\mathrm{s}_{\psi_2}\mathrm{c}_{\phi_2} - \mathrm{c}_{\psi_2}\mathrm{s}_{\phi_2} \\ -\mathrm{s}_{\theta_2} & \mathrm{c}_{\theta_2}\mathrm{s}_{\phi_2} & \mathrm{c}_{\theta_2}\mathrm{c}_{\phi_2} \end{bmatrix}$$

$$\boldsymbol{R}_{r_2} = \frac{1}{\mathrm{c}_{\theta_2}} \begin{bmatrix} \mathrm{c}_{\theta_2} & \mathrm{s}_{\phi_2}\mathrm{s}_{\theta_2} & \mathrm{c}_{\phi_2}\mathrm{s}_{\theta_2} \\ 0 & \mathrm{c}_{\phi_2}\mathrm{c}_{\theta_2} & -\mathrm{s}_{\phi_2}\mathrm{c}_{\theta_2} \\ 0 & \mathrm{s}_{\phi_2} & \mathrm{c}_{\phi_2} \end{bmatrix}$$

The vessel's motions compose of 6-DOF: pitch, heave, roll, surge, sway, and yaw. These motions are divided into two categories. The first three movements are induced by sea waves, and the last three ones are caused by propellers and sea waves. Thus, the dynamic equations of the vessel can be obtained as [18, 19]

$$\begin{cases} \dot{u}_2 = \dfrac{m_{22}}{m_{11}} v_2 r_2 - \dfrac{d_{11}}{m_{11}} u_2 + \dfrac{1}{m_{11}} T_x + \dfrac{1}{m_{11}} d_{t_1} \\ \dot{v}_2 = -\dfrac{m_{11}}{m_{22}} u_2 r_2 - \dfrac{d_{22}}{m_{22}} v_2 + \dfrac{1}{m_{22}} T_y + \dfrac{1}{m_{22}} d_{t_2} \\ \dot{w}_2 = \zeta_1 \sin(\vartheta_1 t + \varrho_1) + d_{t_3} \\ \dot{p}_2 = \zeta_2 \sin(\vartheta_2 t + \varrho_2) + d_{s_1} \\ \dot{q}_2 = \zeta_3 \sin(\vartheta_3 t + \varrho_3) + d_{s_2} \\ \dot{r}_2 = \dfrac{m_{11} - m_{22}}{m_{33}} u_2 v_2 - \dfrac{d_{33}}{m_{33}} r_2 + \dfrac{1}{m_{33}} T_z + \dfrac{1}{m_{33}} d_{s_3} \end{cases} \tag{5}$$

where m_{ii} are given by the vessel inertia and the added mass effects, d_{ii} are given by the hydrodynamic damping. m_{ii} and d_{ii} $(i = 1, 2, 3)$ are assumed to be constant. T_x, T_y, and T_z are the control forces and moment given by propellers. ζ_i and ϑ_i $(i = 1, 2, 3)$ are the motion coefficients depending on the sea conditions. ζ_i represent the amplitude of the sea wave, ϑ_i the frequency, and ι_i the initial phase. To take place some sort of randomisation, ϱ_i are selected randomly. $\boldsymbol{d}_t = [d_{t_1}, d_{t_2}, d_{t_3}]^{\mathrm{T}}$ and $\boldsymbol{d}_s = [d_{s_1}, d_{s_2}, d_{s_3}]^{\mathrm{T}}$ are unknown bounded external disturbances.

Remark 1: The pitch, heave, and roll motions of the vessel are approximated by the sea wave model. This is a commonly used approximation for vessel motion when the absolute details of the vessel motion itself are not the focus of the study. This form of motion can provide a good enough approximation to the vessel conditions [18].

3.3 Relative motion model

According to the models proposed in the above subsection, the relative kinematics are presented as

$$\begin{cases} \dot{\boldsymbol{\xi}} = \boldsymbol{R}_{t_1} \boldsymbol{V} \\ \dot{\boldsymbol{\eta}} = \boldsymbol{R}_{r_1} \boldsymbol{\Omega} \end{cases} \tag{6}$$

where $\boldsymbol{\xi} = \boldsymbol{\xi}_1 - \boldsymbol{\xi}_2 = [x, y, z]^{\mathrm{T}}$ and $\boldsymbol{\eta} = \boldsymbol{\eta}_1 - \boldsymbol{\eta}_2$ are the relative position and relative attitude in $\mathcal{F}_e$, respectively. $\boldsymbol{V} = \boldsymbol{V}_1 - \boldsymbol{R}_{t_{12}} \boldsymbol{V}_2$ and $\boldsymbol{\Omega} = \boldsymbol{\Omega}_1 - \boldsymbol{R}_{r_{12}} \boldsymbol{\Omega}_2$ are the relative velocity and relative angular velocity in $\mathcal{F}_q$, where $\boldsymbol{R}_{t_{12}} = \boldsymbol{R}_{t_1}^{-1} \boldsymbol{R}_{t_2} = \boldsymbol{R}_{t_1}^{\mathrm{T}} \boldsymbol{R}_{t_2}$, $\boldsymbol{R}_{r_{12}} = \boldsymbol{R}_{r_1}^{-1} \boldsymbol{R}_{r_2}$.

The relative dynamics can be expressed as

$$\begin{cases} m_1 \ddot{\boldsymbol{\xi}} = h(\boldsymbol{\eta}_1) F_{\text{total}} - \boldsymbol{K}_t \dot{\boldsymbol{\xi}}_1 + \boldsymbol{R}_{t_1} \boldsymbol{d}_f \\ \qquad - m_1 (\boldsymbol{g} + \dot{\boldsymbol{R}}_{t_2} \boldsymbol{V}_2 + \boldsymbol{R}_{t_2} \dot{\boldsymbol{V}}_2) \\ \boldsymbol{I}_1 \dot{\boldsymbol{\Omega}} = -(\boldsymbol{S}(\boldsymbol{\Omega}_1) \boldsymbol{I}_1 + \boldsymbol{K}_r) \boldsymbol{\Omega}_1 + \boldsymbol{\tau} + \boldsymbol{d}_m \\ \qquad - \boldsymbol{I}_1 (\dot{\boldsymbol{R}}_{r_{12}} \boldsymbol{\Omega}_2 + \boldsymbol{R}_{r_{12}} \dot{\boldsymbol{\Omega}}_2) \end{cases} \tag{7}$$

3.4 Control objective

Define $\Delta F_{\text{total}} = F_{\text{total}} - F_{\text{total0}}$ and $\Delta \boldsymbol{\tau} = \boldsymbol{\tau} - \boldsymbol{\tau}_0$. Then, the model (7) changes to

$$\begin{cases} m_1 \ddot{\boldsymbol{\xi}} = h(\boldsymbol{\eta}_1) F_{\text{total0}} - \boldsymbol{K}_t \dot{\boldsymbol{\xi}}_1 + \boldsymbol{d}_1 \\ \qquad - m_1 (\boldsymbol{g} + \dot{\boldsymbol{R}}_{t_2} \boldsymbol{V}_2 + \boldsymbol{R}_{t_2} \bar{\boldsymbol{V}}_2) \\ \boldsymbol{I}_1 \dot{\boldsymbol{\Omega}} = -(\boldsymbol{S}(\boldsymbol{\Omega}_1) \boldsymbol{I}_1 + \boldsymbol{K}_r) \boldsymbol{\Omega}_1 + \boldsymbol{\tau}_0 + \boldsymbol{d}_2 \\ \qquad - \boldsymbol{I}_1 (\dot{\boldsymbol{R}}_{\boldsymbol{r_{12}}} \boldsymbol{\Omega}_2 + \boldsymbol{R}_{r_{12}} \bar{\boldsymbol{\Omega}}_2) \end{cases} \tag{8}$$

with the lumped disturbances

$$\begin{cases} \boldsymbol{d}_1 = h(\boldsymbol{\eta}_1) \Delta F_{\text{total}} + \boldsymbol{R}_{t_1} \boldsymbol{d}_f - m_1 \boldsymbol{R}_{t_2} \boldsymbol{d}_t \\ \boldsymbol{d}_2 = \Delta \boldsymbol{\tau} + \boldsymbol{d}_m - \boldsymbol{I}_1 \boldsymbol{R}_{r_{12}} \boldsymbol{d}_s \end{cases}$$

where

$$\boldsymbol{d}_t = \left[\frac{d_{t_1}}{m_{11}}, \frac{d_{t_2}}{m_{22}}, d_{t_3} \right]^{\mathrm{T}}, \quad \boldsymbol{d}_s = \left[d_{s_1}, d_{s_2}, \frac{d_{s_3}}{m_{33}} \right]^{\mathrm{T}},$$

$$\bar{\boldsymbol{V}}_2 = [\bar{u}_2, \bar{v}_2, \bar{w}_2]^{\mathrm{T}}, \quad \bar{\boldsymbol{\Omega}}_2 = [\bar{p}_2, \bar{q}_2, \bar{r}_2]^{\mathrm{T}},$$

$$\bar{u}_2 = \frac{m_{22}}{m_{11}} v_2 r_2 - \frac{d_{11}}{m_{11}} u_2 + \frac{T_x}{m_{11}},$$

$$\bar{v}_2 = -\frac{m_{11}}{m_{22}} u_2 r_2 - \frac{d_{22}}{m_{22}} v_2 + \frac{T_y}{m_{22}}, \quad \bar{w}_2 = \zeta_1 \sin(\kappa_1 t + \iota_1),$$

$$\bar{p}_2 = \zeta_2 \sin(\kappa_2 t + \iota_2),$$

$$\bar{q}_2 = \zeta_3 \sin(\kappa_3 t + \iota_3), \quad \bar{r}_2 = \frac{m_{11} - m_{22}}{m_{33}} u_2 v_2 - \frac{d_{33}}{m_{33}} r_2 + \frac{T_z}{m_{33}}.$$

Consider the control saturation constraints, the control inputs F_{total} and $\boldsymbol{\tau}$ are constructed as

$$F_{\text{total}} = \text{sat}(F_{\text{total0}}) \quad \boldsymbol{\tau} = \text{Sat}(\boldsymbol{\tau}_0) \tag{9}$$

where F_{total0} and $\boldsymbol{\tau}_0$ are the control inputs to be designed. For the subsequent developement of control laws, the following assumptions are made.

Assumption 1: The quadrotor is rigid body and symmetrical with respect to the axes $\boldsymbol{x}_q, \boldsymbol{y}_q, \boldsymbol{z}_q$. The mass m_1 is an unknown constant. $\boldsymbol{K}_r$, $\boldsymbol{K}_r$, and $\boldsymbol{I}_1$ are unknown constant unknown matrices.

Assumption 2: The vessel is rigid body and its all states are bounded under the effect of the inputs.

Assumption 3: The Eular angles of the quadrotor are bounded as $\phi_1 \in (-\frac{\pi}{2}, \frac{\pi}{2})$ and $\theta_1 \in (-\frac{\pi}{2}, \frac{\pi}{2})$.

Assumption 4: The lump disturbances $\boldsymbol{d}_1$ and $\boldsymbol{d}_2$ are continuous and bounded by unknown constant bounds, namely $\| \boldsymbol{d}_1 \| \leq \gamma_{d_1}$ and $\| \boldsymbol{d}_2 \| \leq \gamma_{d_2}$, respectively.

The sysytem for the vessel landing of a quadrotor is formulated by (6) and (7). The control objective is to design control inputs F_{total0} and $\boldsymbol{\tau}_0$ such that the quadrotor can land on the vessel steadily in presence of parameter uncertainty, external disturbances, and input saturation. To deal with the underactuated property of the relative system, controller design is divided to two phases: RPC design and RAC design. In the first phase, RPC is designed to coverage the state $\boldsymbol{\xi}$ to $[0, 0, z_d]^{\mathrm{T}}$, and the tracking errors are bounded, where z_d is a known constant. In the second phase, RAC is designed to coverage the states z and $\boldsymbol{\Omega}$ to a small neighbourhood of zero.

4 Control algorithm design

In this section, detailed control algorithm design procedures are presented based on the adaptive sliding mode technique.

4.1 Design of RPC

RPC is designed for the approaching phase which aimed at controlling the quadrotor to fly from afar to above the vessel. Hence, the relative position $\boldsymbol{\xi}$ is desired to coverage to $\boldsymbol{\xi}_d = [0, 0, z_d]^{\mathrm{T}}$ under the control of RPC. In consideration of the strong coupled property of the quadrotor, inner-outer loop design is introduced.

Remark 2: The outer-loop refers to the position control while the inner-loop refers to the attitude control. Reference attitude extraction is applied to connect the two loops. Then, the second-order command filter is employed to elimate the time scale separation assumption between attitude and linear dynamics [33].

(1) *Relative position control design*

First define a sliding variable

$$\boldsymbol{s}_1 = \Delta\dot{\boldsymbol{\xi}} + k_1 \Delta\boldsymbol{\xi} \tag{10}$$

where $\Delta\boldsymbol{\xi} = \boldsymbol{\xi} - \boldsymbol{\xi}_d$. Taking the first derivative of (10) yield

$$\dot{\boldsymbol{s}}_1 = \ddot{\boldsymbol{\xi}} + k_1 \dot{\boldsymbol{\xi}} \tag{11}$$

To separate the unknown parameters from non-linear terms, define a linear operator L. For any vector $\boldsymbol{a} = [a_1, a_2, a_3]^{\mathrm{T}} \in \mathbb{R}^3$, L is defined as $L(\boldsymbol{a}) = \mathrm{diag}\{a_1, a_2 . a_3\}$. Then, we can obtain the following equation from (6), (8), and parameter linearisation

$$\begin{aligned} m_1 \dot{\boldsymbol{s}}_1 &= m_1 \ddot{\boldsymbol{\xi}} + m_1 k_1 \dot{\boldsymbol{\xi}} \\ &= h(\boldsymbol{\eta}_1) F_{\text{total0}} - \boldsymbol{K}_t \boldsymbol{R}_{t_1} \boldsymbol{V}_1 + m_1 \boldsymbol{\Phi}_1 + \boldsymbol{d}_1 \\ &= h(\boldsymbol{\eta}_1) F_{\text{total0}} + \boldsymbol{F}_1 \boldsymbol{\sigma} + m_1 \boldsymbol{\Phi}_1 + \boldsymbol{d}_1 \end{aligned} \tag{12}$$

where $\boldsymbol{\sigma} = [k_{t_1}, k_{t_2}, k_{t_3}]^{\mathrm{T}}$, $\boldsymbol{F}_1 = -L(\boldsymbol{R}_{t_1} \boldsymbol{V}_1)$, $\boldsymbol{\Phi}_1 = (\boldsymbol{k}_1 \dot{\boldsymbol{\xi}} - \boldsymbol{g} - \dot{\boldsymbol{R}}_{t_2} \boldsymbol{V}_2 - \boldsymbol{R}_{t_2} \dot{\bar{\boldsymbol{V}}}_2)$.

Design the product of the item $h(\boldsymbol{\eta}_1)$ and control input as

$$h(\boldsymbol{\eta}_1) F_{\text{total0}} = -k_2 \boldsymbol{s}_1 + k_{c_1} \delta_1 - \boldsymbol{F}_1 \hat{\boldsymbol{\sigma}} - \boldsymbol{\Phi}_1 \hat{m}_1 - \boldsymbol{\gamma}_1 \tag{13}$$

$$\boldsymbol{\gamma}_1 = \begin{cases} \hat{\gamma}_{d_1} \dfrac{\boldsymbol{s}_1}{\| \boldsymbol{s}_1 \|} & \text{if } \hat{\gamma}_{d_1} \| \boldsymbol{s}_1 \| > \kappa_1 \\ \hat{\gamma}_{d_1}^2 \dfrac{\boldsymbol{s}_1}{\kappa_1} & \text{if } \hat{\gamma}_{d_1} \| \boldsymbol{s}_1 \| \leq \kappa_1 \end{cases} \tag{14}$$

and the adaptation laws

$$\begin{cases} \dot{\hat{\boldsymbol{\sigma}}} = k_\sigma (\boldsymbol{F}_1^{\mathrm{T}} \boldsymbol{s}_1 - \beta_\sigma \hat{\boldsymbol{\sigma}}) \\ \dot{\hat{m}}_1 = k_m (\boldsymbol{\Phi}_1^{\mathrm{T}} \boldsymbol{s}_1 - \beta_m \hat{m}_1) \\ \dot{\hat{\gamma}}_{d_1} = k_{d_1} (\| \boldsymbol{s}_1 \| - \beta_{d_1} \hat{\boldsymbol{\gamma}}_{d_1}) \end{cases} \tag{15}$$

where $\hat{\boldsymbol{\sigma}}$ is the estimate of $\boldsymbol{\sigma}$, $\hat{m}_1$ is the estimate of m_1, $\hat{\gamma}_{d_1}$ is the estimate of γ_{d_1}, $k_i (i = 1, 2, c_1, \sigma, m, d_1)$ and $\beta_j (j = \sigma, m, d_1)$ are positive constants, $\kappa_1 > 0$ is the boundary layer. δ_1 is the output of anti-windup saturation compensator [34] designed as

$$\dot{\delta}_1 = -k_{c_2} \delta_1 + \Delta F_{\text{total}} \tag{16}$$

where k_{c_2} is a positive constant.

The control input can be expressed as

$$F_{\text{total0}} = \frac{\Pi_3}{\cos\theta_1 \cos\phi_1}. \tag{17}$$

Besides, (13) can be rewritten as

$$\begin{cases} \sin\theta_1 \cos\psi_1 \cos\phi_1 + \sin\psi_1 \sin\phi_1 = \dfrac{\Pi_1}{F_{\text{total0}}} \\ \sin\theta_1 \sin\psi_1 \cos\phi_1 - \cos\psi_1 \sin\phi_1 = \dfrac{\Pi_2}{F_{\text{total0}}} \end{cases} \tag{18}$$

where Π_1, Π_2, and Π_3 are the first, second, and third elements of $h(\boldsymbol{\eta}_1) F_{\text{total0}}$, respectively. Hence, the attitude-commanded inputs to the inner loop can be computed from (18). The expressions for desired pitch and roll are

$$\begin{cases} \phi_{1d} = \arcsin\left(\dfrac{\Pi_1 \sin\psi_{1d} - \Pi_2 \cos\psi_{1d}}{F_{\text{total0}}} \right) \\ \theta_{1d} = \arcsin\left(\dfrac{\Pi_1 \cos\psi_{1d} + \Pi_2 \sin\psi_{1d}}{F_{\text{total0}} \cos\phi_{1d}} \right) \end{cases} \tag{19}$$

where ψ_{1d} is the commanded yaw attitude.

(2) *Attitude control design*

Define a sliding variable

$$\boldsymbol{s}_2 = \Delta\dot{\boldsymbol{\eta}} + k_3 \Delta\boldsymbol{\eta} \tag{20}$$

where k_3 is a positive constant, $\Delta\boldsymbol{\eta} = \boldsymbol{\eta}_1 - \boldsymbol{\eta}_{1d}$, $\boldsymbol{\eta}_{1d} = [\phi_{1d}, \theta_{1d}, \psi_{1d}]^{\mathrm{T}}$, ϕ_{1d} and θ_{1d} are extracted by (19).

Remark 3: It is worth noting that the controlled variable of inner loop is the attitude of quadrotor rather than relative attitude.

The time derivative of (20) is obtained as

$$\dot{\boldsymbol{s}}_2 = \Delta\ddot{\boldsymbol{\eta}} + k_3 \Delta\dot{\boldsymbol{\eta}} \tag{21}$$

From (6), (7), and parameter linearisation, we can derive

$$
\begin{aligned}
\boldsymbol{I}_1\frac{\mathrm{d}}{\mathrm{d}t}(\boldsymbol{R}_{r_1}^{-1}\boldsymbol{s}_2) &= \boldsymbol{I}_1(\boldsymbol{R}_{r_1}^{-1}\dot{\boldsymbol{s}}_2+\dot{\boldsymbol{R}}_{r_1}^{-1}\boldsymbol{s}_2)\\
&= \boldsymbol{I}_1\boldsymbol{R}_{r_1}^{-1}[(\ddot{\boldsymbol{\eta}}_1-\ddot{\boldsymbol{\eta}}_{1d})+k_3(\dot{\boldsymbol{\eta}}_1-\dot{\boldsymbol{\eta}}_{1d})]\\
&\quad +\boldsymbol{I}_1\dot{\boldsymbol{R}}_{r_1}{}^{-1}[(\dot{\boldsymbol{\eta}}_1-\dot{\boldsymbol{\eta}}_{1d})+k_3(\boldsymbol{\eta}_1-\boldsymbol{\eta}_{1d})]\\
&= \boldsymbol{I}_1\dot{\boldsymbol{\Omega}}_1-\boldsymbol{I}_1\boldsymbol{R}_{r_1}^{-1}\ddot{\boldsymbol{\eta}}_{1d}+\boldsymbol{I}_1\boldsymbol{R}_{r_1}^{-1}k_3(\dot{\boldsymbol{\eta}}_1-\dot{\boldsymbol{\eta}}_{1d})\\
&\quad -\boldsymbol{I}_1\dot{\boldsymbol{R}}_{r_1}{}^{-1}\dot{\boldsymbol{\eta}}_{1d}+\boldsymbol{I}_1\dot{\boldsymbol{R}}_{r_1}{}^{-1}k_3(\boldsymbol{\eta}_1-\boldsymbol{\eta}_{1d})\\
&= \boldsymbol{F}_2\boldsymbol{\epsilon}+\boldsymbol{\Phi}_2\boldsymbol{I}_m+\boldsymbol{\tau}_0+\boldsymbol{d}_2
\end{aligned}
\tag{22}
$$

where $\boldsymbol{\epsilon}=[k_{r_1},k_{r_2},k_{r_3}]^{\mathrm{T}}$, $\boldsymbol{I}_m=[I_x,I_y,I_z]^{\mathrm{T}}$, $\boldsymbol{F}_2=-L(\boldsymbol{\Omega}_1)$, $\boldsymbol{\Phi}_2=-\boldsymbol{S}(\boldsymbol{\Omega}_1)L(\boldsymbol{\Omega}_1)+L[\boldsymbol{R}_{r_1}^{-1}k_3(\dot{\boldsymbol{\eta}}_1-\dot{\boldsymbol{\eta}}_{1d})]+L[\dot{\boldsymbol{R}}_{r_1}{}^{-1}k_3(\boldsymbol{\eta}_1-\boldsymbol{\eta}_{1d})]$ $-L(\boldsymbol{R}_{r_1}^{-1}\ddot{\boldsymbol{\eta}}_{1d})-L(\dot{\boldsymbol{R}}_{r_1}^{-1}\dot{\boldsymbol{\eta}}_{1d})$.

Although the commanded attitude $\boldsymbol{\eta}_{1d}$ is known, the computation of the first derivative and the second derivative is extremely intricate and dependent on analytic model. In this case, a second-order command filter is adopted to obtain the derivative [35]

$$
\begin{cases}
\dot{\boldsymbol{X}}_1=\boldsymbol{X}_2\\
\dot{\boldsymbol{X}}_2=-2\Lambda\omega_n\boldsymbol{X}_2-\omega_n^2(\boldsymbol{X}_1-\boldsymbol{\eta}_{1d})
\end{cases}
\tag{23}
$$

where Λ is the damping ratio and ω_n is the damping frequency. Define the output of command filter $\hat{\boldsymbol{\eta}}_{1d}\triangleq\boldsymbol{X}_2$, $\dot{\hat{\boldsymbol{\eta}}}_{1d}\triangleq\dot{\boldsymbol{X}}_2$. Therefore, (22) can be rewritten as

$$
\boldsymbol{I}_1\frac{\mathrm{d}}{\mathrm{d}t}(\boldsymbol{R}_{r_1}^{-1}\boldsymbol{s}_2)=\boldsymbol{F}_2\boldsymbol{\epsilon}+\hat{\boldsymbol{\Phi}}_2\boldsymbol{I}_m+\boldsymbol{\tau}_0+\boldsymbol{d}_2^*
\tag{24}
$$

where $\hat{\boldsymbol{\Phi}}_2=-\boldsymbol{S}(\boldsymbol{\Omega}_1)L(\boldsymbol{\Omega}_1)+L[\boldsymbol{R}_{r_1}^{-1}k_3(\dot{\boldsymbol{\eta}}_1-\dot{\hat{\boldsymbol{\eta}}}_{1d})]+L[\dot{\boldsymbol{R}}_{r_1}{}^{-1}k_3(\boldsymbol{\eta}_1-\boldsymbol{\eta}_{1d})]-L(\boldsymbol{R}_{r_1}^{-1}\ddot{\hat{\boldsymbol{\eta}}}_{1d})-L(\dot{\boldsymbol{R}}_{r_1}^{-1}\dot{\hat{\boldsymbol{\eta}}}_{1d})$, $\boldsymbol{d}_2^*=\boldsymbol{d}_2+(\boldsymbol{\Phi}_2-\hat{\boldsymbol{\Phi}}_2)\boldsymbol{I}_m$.

Remark 4: Setting large enough ω_n and appropriate Λ can guarantee the fast tracking to commanded attitude derivative signal, that is, the error $\boldsymbol{\Phi}_2-\hat{\boldsymbol{\Phi}}_2$ is bounded. Thus, $\boldsymbol{d}_2^*$ is also bounded by an unknown constant, namely $\|\boldsymbol{d}_2^*\|\le\gamma_{d_2}^*$.

Design the attitude control input

$$
\boldsymbol{\tau}_0=-k_4\boldsymbol{R}_{r_1}^{-1}\boldsymbol{s}_2+k_{c_3}\boldsymbol{\delta}_2-\hat{\boldsymbol{\Phi}}_2\hat{\boldsymbol{I}}_m-\boldsymbol{F}_2\hat{\boldsymbol{\epsilon}}-\boldsymbol{\gamma}_2
\tag{25}
$$

$$
\boldsymbol{\gamma}_2=\begin{cases}
\hat{\gamma}_{d_2}^*\dfrac{\boldsymbol{R}_{r_1}^{-1}\boldsymbol{s}_2}{\|\boldsymbol{R}_{r_1}^{-1}\boldsymbol{s}_2\|} & \text{if } \hat{\gamma}_{d_2}^*\|\boldsymbol{R}_{r_1}^{-1}\boldsymbol{s}_2\|>\kappa_2\\
\hat{\gamma}_{d_2}^{*2}\dfrac{\boldsymbol{R}_{r_1}^{-1}\boldsymbol{s}_2}{\kappa_2} & \text{if } \hat{\gamma}_{d_2}^*\|\boldsymbol{R}_{r_1}^{-1}\boldsymbol{s}_2\|\le\kappa_2
\end{cases}
\tag{26}
$$

and the adaptation laws

$$
\begin{cases}
\dot{\hat{\boldsymbol{\epsilon}}}=k_\epsilon[\boldsymbol{F}_2^{\mathrm{T}}(\boldsymbol{R}_{r_1}^{-1}\boldsymbol{s}_2)-\beta_\epsilon\hat{\boldsymbol{\epsilon}}]\\
\dot{\hat{\boldsymbol{I}}}_m=k_I[\hat{\boldsymbol{\Phi}}_2^{\mathrm{T}}(\boldsymbol{R}_{r_1}^{-1}\boldsymbol{s}_2)-\beta_I\hat{\boldsymbol{I}}_m]\\
\dot{\hat{\gamma}}_{d_2}^*=k_{d_2}(\|\boldsymbol{R}_{r_1}^{-1}\boldsymbol{s}_2\|-\beta_{d_2}\hat{\gamma}_{d_2}^*)
\end{cases}
\tag{27}
$$

where $\hat{\boldsymbol{\epsilon}}$ is the estimate of $\boldsymbol{\epsilon}$, $\hat{\boldsymbol{I}}_m$ is the estimate of $\boldsymbol{I}_m$, $\hat{\gamma}_{d_2}^*$ is the estimate of $\gamma_{d_2}^*$, $k_i(i=4,c_3,\epsilon,I,d_2)$ and $\beta_j(j=\epsilon,I,d_2)$ are positive contants, $\kappa_2>0$ is the boundary layer. $\boldsymbol{\delta}_2$ is the output of anti-windup saturation compensator designed as

$$
\dot{\boldsymbol{\delta}}_2=-k_{c_4}\boldsymbol{\delta}_2+\Delta\boldsymbol{\tau}
\tag{28}
$$

where k_{c_4} is a positive constant.

Theorem 1: For the relative motion of the quadrotor and vessel system (6) and (7) with input saturation (9) under Assumptions 1–4, the proposed RPC (15), (17), (25), and (27) under $2k_2>k_{c_1}$, $2k_4>k_{c_3}$, $2k_{c_2}>k_{c_1}+1$, and $2k_{c_4}>k_{c_3}+1$ can guarantee that the relative position error $\Delta\boldsymbol{\xi}$ and the attitude error of the quadrotor $\Delta\boldsymbol{\eta}$ converge to a small neighbourhood of zero.

Proof: Define the estimate errors $\tilde{\boldsymbol{\sigma}}=\hat{\boldsymbol{\sigma}}-\boldsymbol{\sigma}$, $\tilde{m}_1=\hat{m}_1-m_1$, $\tilde{\gamma}_{d_1}=\hat{\gamma}_{d_1}-\gamma_{d_1}$, $\tilde{\boldsymbol{\epsilon}}=\hat{\boldsymbol{\epsilon}}-\boldsymbol{\epsilon}$, $\tilde{\boldsymbol{I}}_m=\hat{\boldsymbol{I}}_m-\boldsymbol{I}_m$, $\tilde{\gamma}_{d_2}^*=\hat{\gamma}_{d_2}^*-\gamma_{d_2}^*$, respectively.

Considering the Lyapunov function candidate as

$$
V_m=V_s+V_t
\tag{29}
$$

where

$$
\begin{aligned}
V_s&=\frac{1}{2}m_1\boldsymbol{s}_1^{\mathrm{T}}\boldsymbol{s}_1+\frac{1}{2}\delta_1^2+\frac{1}{2k_\sigma}\tilde{\boldsymbol{\sigma}}^{\mathrm{T}}\tilde{\boldsymbol{\sigma}}+\frac{1}{2k_m}\tilde{m}_1^2+\frac{1}{2k_{d_1}}\tilde{\gamma}_{d_1}^2\\
V_t&=\frac{1}{2}(\boldsymbol{R}_{r_1}^{-1}\boldsymbol{s}_2)^{\mathrm{T}}\boldsymbol{I}_1(\boldsymbol{R}_{r_1}^{-1}\boldsymbol{s}_2)+\frac{1}{2}\boldsymbol{\delta}_2^T\boldsymbol{\delta}_2+\frac{1}{2k_I}\tilde{\boldsymbol{I}}_m^{\mathrm{T}}\tilde{\boldsymbol{I}}_m\\
&\quad +\frac{1}{2k_\epsilon}\tilde{\boldsymbol{\epsilon}}^{\mathrm{T}}\tilde{\boldsymbol{\epsilon}}+\frac{1}{2k_{d_2}}\tilde{\gamma}_{d_2}^{*2}
\end{aligned}
$$

Differentiating (29) with respect to time yields

$$
\begin{aligned}
\dot{V}_m&=m_1\boldsymbol{s}_1^{\mathrm{T}}\dot{\boldsymbol{s}}_1+\frac{1}{k_\sigma}\tilde{\boldsymbol{\sigma}}^{\mathrm{T}}\dot{\tilde{\boldsymbol{\sigma}}}+\frac{1}{k_m}\tilde{m}_1\dot{\tilde{m}}_1+\frac{1}{k_{d_1}}\tilde{\gamma}_{d_1}\dot{\tilde{\gamma}}_{d_1}\\
&\quad +\delta_1\dot{\delta}_1+(\boldsymbol{R}_{r_1}^{-1}\boldsymbol{s}_2)^{\mathrm{T}}\boldsymbol{I}_1\frac{\mathrm{d}}{\mathrm{d}t}(\boldsymbol{R}_{r_1}^{-1}\boldsymbol{s}_2)+\frac{1}{k_\epsilon}\tilde{\boldsymbol{\epsilon}}^{\mathrm{T}}\dot{\tilde{\boldsymbol{\epsilon}}}\\
&\quad +\frac{1}{k_I}\tilde{\boldsymbol{I}}_m^{\mathrm{T}}\dot{\tilde{\boldsymbol{I}}}_m+\frac{1}{k_{d_2}}\tilde{\gamma}_{d_2}^*\dot{\tilde{\gamma}}_{d_2}^*+\boldsymbol{\delta}_2^T\dot{\boldsymbol{\delta}}_2
\end{aligned}
\tag{30}
$$

With (12), (13), (16), (24), (25), and (28), (30) can be derived as

$$
\begin{aligned}
\dot{V}_m&=\boldsymbol{s}_1^{\mathrm{T}}(h(\boldsymbol{\eta}_1)F_{\mathrm{total}0}+\boldsymbol{F}_1\boldsymbol{\sigma}+m_1\boldsymbol{\Phi}_1+\boldsymbol{d}_1)+\frac{1}{k_\sigma}\tilde{\boldsymbol{\sigma}}^{\mathrm{T}}\dot{\tilde{\boldsymbol{\sigma}}}\\
&\quad +\frac{1}{k_m}\tilde{m}_1\dot{\tilde{m}}_1+\frac{1}{k_{d_1}}\tilde{\gamma}_{d_1}\dot{\tilde{\gamma}}_{d_1}-k_{c_2}\delta_1^2+\delta_1\Delta F_{\mathrm{total}}\\
&\quad +(\boldsymbol{R}_{r_1}^{-1}\boldsymbol{s}_2)^{\mathrm{T}}(\boldsymbol{F}_2\boldsymbol{\epsilon}+\hat{\boldsymbol{\Phi}}_2\boldsymbol{I}_m+\boldsymbol{\tau}_0+\boldsymbol{d}_2^*)+\frac{1}{k_\epsilon}\tilde{\boldsymbol{\epsilon}}^{\mathrm{T}}\dot{\tilde{\boldsymbol{\epsilon}}}\\
&\quad +\frac{1}{k_I}\tilde{\boldsymbol{I}}_m^{\mathrm{T}}\dot{\tilde{\boldsymbol{I}}}_m+\frac{1}{k_{d_2}}\tilde{\gamma}_{d_2}^*\dot{\tilde{\gamma}}_{d_2}^*-k_{c_4}\boldsymbol{\delta}_2^{\mathrm{T}}\boldsymbol{\delta}_2+\boldsymbol{\delta}_2^{\mathrm{T}}\Delta\boldsymbol{\tau}\\
&=-k_2\boldsymbol{s}_1^{\mathrm{T}}\boldsymbol{s}_1+k_{c_1}\boldsymbol{s}_1^{\mathrm{T}}\delta_1-\boldsymbol{s}_1^{\mathrm{T}}\boldsymbol{F}_1\tilde{\boldsymbol{\sigma}}-\boldsymbol{s}_1^{\mathrm{T}}\boldsymbol{\Phi}_1\tilde{m}_1+\boldsymbol{s}_1^{\mathrm{T}}\boldsymbol{d}_1\\
&\quad -\boldsymbol{s}_1^{\mathrm{T}}\boldsymbol{\gamma}_1+\frac{1}{k_\sigma}\tilde{\boldsymbol{\sigma}}^{\mathrm{T}}\dot{\tilde{\boldsymbol{\sigma}}}+\frac{1}{k_m}\tilde{m}_1\dot{\tilde{m}}_1+\frac{1}{k_{d_1}}\tilde{\gamma}_{d_1}\dot{\tilde{\gamma}}_{d_1}\\
&\quad -k_{c_2}\delta_1^2+\delta_1\Delta F_{\mathrm{total}}-k_4(\boldsymbol{R}_{r_1}^{-1}\boldsymbol{s}_2)^{\mathrm{T}}(\boldsymbol{R}_{r_1}^{-1}\boldsymbol{s}_2)\\
&\quad +k_{c_3}(\boldsymbol{R}_{r_1}^{-1}\boldsymbol{s}_2)^{\mathrm{T}}\boldsymbol{\delta}_2-(\boldsymbol{R}_{r_1}^{-1}\boldsymbol{s}_2)^{\mathrm{T}}\boldsymbol{F}_2\tilde{\boldsymbol{\epsilon}}+\frac{1}{k_\epsilon}\tilde{\boldsymbol{\epsilon}}^{\mathrm{T}}\dot{\tilde{\boldsymbol{\epsilon}}}\\
&\quad +(\boldsymbol{R}_{r_1}^{-1}\boldsymbol{s}_2)^{\mathrm{T}}\boldsymbol{d}_2^*-(\boldsymbol{R}_{r_1}^{-1}\boldsymbol{s}_2)^{\mathrm{T}}\boldsymbol{\gamma}_2-(\boldsymbol{R}_{r_1}^{-1}\boldsymbol{s}_2)^{\mathrm{T}}\hat{\boldsymbol{\Phi}}_2\tilde{\boldsymbol{I}}_m\\
&\quad +\frac{1}{k_I}\tilde{\boldsymbol{I}}_m^{\mathrm{T}}\dot{\tilde{\boldsymbol{I}}}_m+\frac{1}{k_{d_2}}\tilde{\gamma}_{d_2}^*\dot{\tilde{\gamma}}_{d_2}^*-k_{c_4}\boldsymbol{\delta}_2^{\mathrm{T}}\boldsymbol{\delta}_2+\boldsymbol{\delta}_2^{\mathrm{T}}\Delta\boldsymbol{\tau}
\end{aligned}
\tag{31}
$$

Notice the properties $\boldsymbol{s}_1^{\mathrm{T}}\boldsymbol{d}_1\le\gamma_{d_1}\|\boldsymbol{s}_1\|$ and $(\boldsymbol{R}_{r_1}^{-1}\boldsymbol{s}_2)^{\mathrm{T}}\boldsymbol{d}_2^*\le\gamma_{d_2}^*\|\boldsymbol{R}_{r_1}^{-1}\boldsymbol{s}_2\|$, if $\hat{\gamma}_{d_1}\|\boldsymbol{s}_1\|>\kappa_1$ and $\hat{\gamma}_{d_2}^*\|\boldsymbol{R}_{r_1}^{-1}\boldsymbol{s}_2\|>\kappa_2$, (31) can be rewritten as

$$
\begin{aligned}
\dot{V}_m \le & -k_2 \boldsymbol{s}_1^{\mathrm{T}}\boldsymbol{s}_1 + k_{c_1}\boldsymbol{s}_1^{\mathrm{T}}\delta_1 - \boldsymbol{s}_1^{\mathrm{T}}\boldsymbol{F}_1\tilde{\boldsymbol{\sigma}} - \boldsymbol{s}_1^{\mathrm{T}}\boldsymbol{\Phi}_1\tilde{m}_1 \\
& -\tilde{\gamma}_{d_1} \parallel \boldsymbol{s}_1 \parallel + \frac{1}{k_\sigma}\tilde{\boldsymbol{\sigma}}^{\mathrm{T}}\dot{\tilde{\boldsymbol{\sigma}}} + \frac{1}{k_m}\tilde{m}_1\dot{\tilde{m}}_1 + \frac{1}{k_{d_1}}\tilde{\gamma}_{d_1}\dot{\tilde{\gamma}}_{d_1} \\
& +\delta_1\Delta F_{\mathrm{total}} - k_{c_2}\delta_1^2 - k_4(\boldsymbol{R}_{r_1}^{-1}\boldsymbol{s}_2)^{\mathrm{T}}(\boldsymbol{R}_{r_1}^{-1}\boldsymbol{s}_2) \\
& +k_{c_3}(\boldsymbol{R}_{r_1}^{-1}\boldsymbol{s}_2)^{\mathrm{T}}\boldsymbol{\delta}_2 - (\boldsymbol{R}_{r_1}^{-1}\boldsymbol{s}_2)^{\mathrm{T}}\boldsymbol{F}_2\tilde{\boldsymbol{\epsilon}} \\
& -\tilde{\gamma}_{d_2}^{*} \parallel \boldsymbol{R}_{r_1}^{-1}\boldsymbol{s}_2 \parallel - (\boldsymbol{R}_{r_1}^{-1}\boldsymbol{s}_2)^{\mathrm{T}}\hat{\boldsymbol{\Phi}}_2\tilde{\boldsymbol{I}}_m + \frac{1}{k_\epsilon}\tilde{\boldsymbol{\epsilon}}^{\mathrm{T}}\dot{\tilde{\boldsymbol{\epsilon}}} \\
& +\frac{1}{k_I}\tilde{\boldsymbol{I}}_m^{\mathrm{T}}\dot{\tilde{\boldsymbol{I}}}_m + \frac{1}{k_{d_2}}\tilde{\gamma}_{d_2}^{*}\dot{\tilde{\gamma}}_{d_2}^{*} - k_{c_4}\boldsymbol{\delta}_2^{\mathrm{T}}\boldsymbol{\delta}_2 + \boldsymbol{\delta}_2^{\mathrm{T}}\Delta\boldsymbol{\tau}
\end{aligned} \tag{32}
$$

Substituting adaptation laws (15) and (27) into (32) and applying Young inequality [36] yield

$$
\begin{aligned}
\dot{V}_m \le & -k_2\boldsymbol{s}_1^{\mathrm{T}}\boldsymbol{s}_1 - k_{c_2}\delta_1^2 + k_{c_1}\boldsymbol{s}_1^{\mathrm{T}}\delta_1 + \delta_1\Delta F_{\mathrm{total}} \\
& -k_4(\boldsymbol{R}_{r_1}^{-1}\boldsymbol{s}_2)^{\mathrm{T}}(\boldsymbol{R}_{r_1}^{-1}\boldsymbol{s}_2) - k_{c_4}\boldsymbol{\delta}_2^{\mathrm{T}}\boldsymbol{\delta}_2 + \boldsymbol{\delta}_2^{\mathrm{T}}\Delta\boldsymbol{\tau} \\
& +k_{c_3}(\boldsymbol{R}_{r_1}^{-1}\boldsymbol{s}_2)^{\mathrm{T}}\boldsymbol{\delta}_2 - \beta_\sigma\tilde{\boldsymbol{\sigma}}^{\mathrm{T}}\hat{\boldsymbol{\sigma}} - \beta_m\tilde{m}_1\hat{m}_1 \\
& -\beta_{d_1}\tilde{\gamma}_{d_1}\hat{\gamma}_{d_1} - \beta_\epsilon\tilde{\boldsymbol{\epsilon}}^{\mathrm{T}}\hat{\boldsymbol{\epsilon}} - \beta_I\tilde{\boldsymbol{I}}_m^{\mathrm{T}}\hat{\boldsymbol{I}}_m - \beta_{d_2}\tilde{\gamma}_{d_2}^{*}\hat{\gamma}_{d_2}^{*} \\
\le & -\left(k_2 - \frac{k_{c_1}}{2}\right) \parallel \boldsymbol{s}_1 \parallel^2 - \frac{2k_{c_2} - k_{c_1} - 1}{2}|\delta_1|^2 - \frac{\beta_\sigma}{2} \parallel \tilde{\boldsymbol{\sigma}} \parallel^2 \\
& -\frac{\beta_m}{2}|\tilde{m}_1|^2 - \frac{\beta_{d_1}}{2}|\tilde{\gamma}_{d_1}|^2 - \left(k_4 - \frac{k_{c_3}}{2}\right) \parallel \boldsymbol{R}_{r_1}^{-1}\boldsymbol{s}_2 \parallel^2 \\
& -\frac{2k_{c_4} - k_{c_3} - 1}{2} \parallel \boldsymbol{\delta}_2 \parallel^2 - \frac{\beta_\epsilon}{2} \parallel \tilde{\boldsymbol{\epsilon}} \parallel^2 - \frac{\beta_I}{2} \parallel \tilde{\boldsymbol{I}}_m \parallel^2 \\
& -\frac{\beta_{d_2}}{2}|\tilde{\gamma}_{d_2}^{*}|^2 + \iota_1
\end{aligned} \tag{33}
$$

where $\iota_1 = (\beta_\sigma/2) \parallel \boldsymbol{\sigma} \parallel^2 + (\beta_m/2)|m_1|^2 + (\beta_{d_1}/2)|\gamma_{d_1}|^2 + (\beta_\epsilon/2) \parallel \boldsymbol{\epsilon} \parallel^2 + (\beta_I/2) \parallel \boldsymbol{I}_m \parallel^2 + (\beta_{d_2}/2)|\gamma_{d_2}^{*}|^2 + \frac{1}{2}|\Delta F_{\mathrm{total}}|^2 + \frac{1}{2} \parallel \Delta\boldsymbol{\tau} \parallel^2$.

If $\hat{\gamma}_{d_1} \parallel \boldsymbol{s}_1 \parallel \le \kappa_1$ and $\hat{\gamma}_{d_2}^{*} \parallel \boldsymbol{R}_{r_1}^{-1}\boldsymbol{s}_2 \parallel \le \kappa_2$, then

$$
\begin{aligned}
\dot{V}_m \le & -k_2\boldsymbol{s}_1^{\mathrm{T}}\boldsymbol{s}_1 - k_{c_2}\delta_1^2 + k_{c_1}\boldsymbol{s}_1^{\mathrm{T}}\delta_1 + \delta_1\Delta F_{\mathrm{total}} \\
& -k_4(\boldsymbol{R}_{r_1}^{-1}\boldsymbol{s}_2)^{\mathrm{T}}(\boldsymbol{R}_{r_1}^{-1}\boldsymbol{s}_2) - k_{c_4}\boldsymbol{\delta}_2^{\mathrm{T}}\boldsymbol{\delta}_2 + \boldsymbol{\delta}_2^{\mathrm{T}}\Delta\boldsymbol{\tau} \\
& +k_{c_3}(\boldsymbol{R}_{r_1}^{-1}\boldsymbol{s}_2)^{\mathrm{T}}\boldsymbol{\delta}_2 - \frac{1}{\kappa_1}\left(\hat{\gamma}_{d_1} \parallel \boldsymbol{s}_1 \parallel - \frac{\kappa_1}{2}\right)^2 + \frac{\kappa_1}{4} \\
& -\frac{1}{\kappa_2}\left(\hat{\gamma}_{d_2}^{*} \parallel \boldsymbol{s}_2 \parallel - \frac{\kappa_2}{2}\right)^2 + \frac{\kappa_2}{4} - \beta_\sigma\tilde{\boldsymbol{\sigma}}^{\mathrm{T}}\hat{\boldsymbol{\sigma}} - \beta_m\tilde{m}_1\hat{m}_1 \\
& -\beta_{d_1}\tilde{\gamma}_{d_1}\hat{\gamma}_{d_1} - \beta_\epsilon\tilde{\boldsymbol{\epsilon}}^{\mathrm{T}}\hat{\boldsymbol{\epsilon}} - \beta_I\tilde{\boldsymbol{I}}_m^{\mathrm{T}}\hat{\boldsymbol{I}}_m - \beta_{d_2}\tilde{\gamma}_{d_2}^{*}\hat{\gamma}_{d_2}^{*} \\
\le & -\left(k_2 - \frac{k_{c_1}}{2}\right) \parallel \boldsymbol{s}_1 \parallel^2 - \frac{2k_{c_2} - k_{c_1} - 1}{2}|\delta_1|^2 - \frac{\beta_\sigma}{2} \parallel \tilde{\boldsymbol{\sigma}} \parallel^2 \\
& -\frac{\beta_m}{2}|\tilde{m}_1|^2 - \frac{\beta_{d_1}}{2}|\tilde{\gamma}_{d_1}|^2 - \left(k_4 - \frac{k_{c_3}}{2}\right) \parallel \boldsymbol{R}_{r_1}^{-1}\boldsymbol{s}_2 \parallel^2 \\
& -\frac{2k_{c_4} - k_{c_3} - 1}{2} \parallel \boldsymbol{\delta}_2 \parallel^2 - \frac{\beta_\epsilon}{2} \parallel \tilde{\boldsymbol{\epsilon}} \parallel^2 - \frac{\beta_I}{2} \parallel \tilde{\boldsymbol{I}}_m \parallel^2 \\
& -\frac{\beta_{d_2}}{2}|\tilde{\gamma}_{d_2}^{*}|^2 + \iota_1^{*}
\end{aligned} \tag{34}
$$

where $\iota_1^{*} = \iota_1 + (\kappa_1/4) + (\kappa_2/4)$.

According to (33) and (34), we have that if $2k_2 > k_{c_1}$, $2k_4 > k_{c_3}$, $2k_{c_2} > k_{c_1} + 1$, and $2k_{c_4} > k_{c_3} + 1$, then $\dot{V}_m \le -\rho_1 V_m + \iota_1^{*}$, where $\rho_1 = \rho_0/\rho_{\max}$,

$$
\rho_0 = \min\left(k_2 - \frac{k_{c_1}}{2}, \frac{2k_{c_2} - k_{c_1} - 1}{2}, \frac{\beta_\sigma}{2}, \frac{\beta_m}{2}, \frac{\beta_{d_1}}{2}, k_4 - \frac{k_{c_3}}{2}, \frac{2k_{c_4} - k_{c_3} - 1}{2}, \frac{\beta_\epsilon}{2}, \frac{\beta_I}{2}, \frac{\beta_{d_2}}{2}\right),
$$

$$
\rho_{\max} = \frac{1}{2}\max\left(m_1, 1, \frac{1}{k_\sigma}, \frac{1}{k_m}, \frac{1}{k_{d_1}}, \lambda_{\max}(\boldsymbol{I}_1), \frac{1}{k_I}, \frac{1}{k_\epsilon}, \frac{1}{k_{d_2}}\right).
$$

Then, applying comparison principle [37], we derive

$$
V_m(t) \le \left(V_m(0) - \frac{\iota_1^{*}}{\rho_1}\right)e^{-\rho_1 t} + \frac{\iota_1^{*}}{\rho_1} \le \frac{\iota_1^{*}}{\rho_1}.
$$

It implies that $\boldsymbol{s}_1$, $\boldsymbol{s}_2$, $\tilde{\boldsymbol{\sigma}}$, $\tilde{m}_1$, $\tilde{\boldsymbol{\epsilon}}$, $\tilde{\boldsymbol{I}}_m$, $\tilde{\gamma}_{d_1}$, $\tilde{\gamma}_{d_2}^{*}$, δ_1, $\boldsymbol{\delta}_2$ are coverage eventually to a small set. Thus, from (10) and (20), we can conclude $\Delta\boldsymbol{\xi}$ and $\Delta\boldsymbol{\eta}$ are coverage to a small neighbourhood of zero. Besides, From (7), (17) and (25), we can conclude that all states of the closed-loop system are bounded. □

Remark 5: In the proof, it should be indicated that the inequation $\dot{V}_m \le -\rho_1 V_m + \iota_1^{*}$ also holds under the condition $\hat{\gamma}_{d_1} \parallel \boldsymbol{s}_1 \parallel > \kappa_1$, $\hat{\gamma}_{d_2}^{*} \parallel \boldsymbol{R}_{r_1}^{-1}\boldsymbol{s}_2 \parallel \le \kappa_2$ or the condition $\hat{\gamma}_{d_1} \parallel \boldsymbol{s}_1 \parallel \le \kappa_1$, $\hat{\gamma}_{d_2}^{*} \parallel \boldsymbol{R}_{r_1}^{-1}\boldsymbol{s}_2 \parallel > \kappa_2$ and it can be proved by the same proof method as aforementioned.

Remark 6: Under the Assumption 4, we know that $|\gamma_{d_1}|$, $|\gamma_{d_2}^{*}|$, $|\Delta F_{\mathrm{total}}|$, and $\parallel \Delta\boldsymbol{\tau} \parallel$ are always bounded, then ι^{*} can be derived bounded, so that $\lim_{t\to\infty} V_m(t) \le \varpi$, where ϖ is an unknown scalar. The convergence boundary ϖ mainly depends on ι_1^{*} and ρ_1, while smaller ι_1^{*} and bigger ρ_1 lead to smaller ϖ. ρ_1 is involved by ρ_0 and $\rho_{\max}$, thereby we should select appropriate control parameters to achieve bigger ρ_0 and smaller $\rho_{\max}$. Meanwhile, smaller κ_1, κ_2 and the differences between the actual actuator output and desired control input result in smaller ϖ.

Remark 7: The states δ_1 and $\boldsymbol{\delta}_2$ in the saturation compensators (16) and (28) are utilised to deal with the infaust effect of input saturation. The differences $\Delta F_{\mathrm{total}}$ and $\Delta\boldsymbol{\tau}$ are fed back to the controllers via the gains k_{c_1} and k_{c_3} to compensate the input saturation.

Remark 8: The piecewise expressions (14) and (26) named boundary layer [38] are applied to offer continuous approximation to the discontinuous sliding mode controllers inside the boundary layers and guarantee the motions within the neighbourhood of the sliding surfaces, thereby remove the undesirable chattering. However, the asymptotically stability cannot be guaranteed under the controller with the boundary layer. Higher order sliding mode control [27, 28] can address the issue, providing a finite-time convergence to the origin, which will be considered in further study.

4.2 Design of RAC

As above, the quadrotor can reach above the vessel under the command of RPC. In this subsection, RAC is proposed to drive the quadrotor descend vertically on the vessel and synchronise the attitude of the quadrotor and vessel simultaneously. In view of the under-actuated property of the quadrotor, we only consider the relative altitude and relative attitude of the quadrotor and vessel in RAC, controlling the position in *Oxy* plane is beyond the scope. Therefore, it should be mentioned the landing phase shall be fast so that the relative positions x and y can be as small as possible.

(1) *Relative altitude control design*

Simplify the relative kinematics (6) and relative dynamics (7), the relative altitude equations are expressed as

$$
\begin{cases}
\dot{z} = \boldsymbol{R}_{t_1}^{3}\boldsymbol{V} \\
\ddot{z} = \dfrac{n(\boldsymbol{\eta}_1)F_{\mathrm{total0}} - k_{t_3}\dot{z}_1 + d_3}{m_1} - (g_s + \dot{\boldsymbol{R}}_{t_2}^{3}\boldsymbol{V}_2 + \boldsymbol{R}_{t_2}^{3}\dot{\bar{\boldsymbol{V}}}_2)
\end{cases} \tag{35}
$$

where $n(\boldsymbol{\eta}_1) = \cos\theta_1\cos\phi_1$. $\boldsymbol{R}_{t_1}^{3}$ and $\boldsymbol{R}_{t_2}^{3}$ are the last row of $\boldsymbol{R}_{t_1}$ and $\boldsymbol{R}_{t_2}$, respectively. $d_3 = n(\boldsymbol{\eta}_1)\Delta F_{\mathrm{total}} + \boldsymbol{R}_{t_1}^{3}\boldsymbol{d}_f - m_1\boldsymbol{R}_{t_2}^{3}\boldsymbol{d}_t$.

Define a sliding variable

$$s_3 = \dot{z} + k_5 z \tag{36}$$

Combining (35), the time derivative of (36) is

$$\begin{aligned} m_1\dot{s}_3 &= m_1\ddot{z} + k_5\dot{z} \\ &= n(\boldsymbol{\eta}_1)F_{\text{total0}} + F_3 k_{t_3} + m_1\Phi_3 + d_3 \end{aligned} \tag{37}$$

where $F_3 = -\boldsymbol{R}_{t_1}^3\boldsymbol{V}_1$, $\Phi_3 = k_5\dot{z} - g_s - \dot{\boldsymbol{R}}_{t_2}^3\boldsymbol{V}_2 - \boldsymbol{R}_{t_2}^3\bar{\boldsymbol{V}}_2$.

Design the relative altitude control input

$$F_{\text{total0}} = \frac{-k_6 s_3 + k_{c_5}\delta_3 - F_3\hat{k}_{t_3} - \Phi_3\hat{m}_1 - \gamma_3}{n(\boldsymbol{\eta}_1)} \tag{38}$$

$$\gamma_3 = \begin{cases} \hat{\gamma}_{d_3}\dfrac{s_3}{|s_3|} & \text{if } \hat{\gamma}_{d_3}|s_3| > \kappa_3 \\ \hat{\gamma}_{d_3}^2\dfrac{s_3}{\kappa_3} & \text{if } \hat{\gamma}_{d_3}|s_3| \le \kappa_3 \end{cases} \tag{39}$$

and the adaptation laws

$$\begin{cases} \dot{\hat{k}}_{t_3} = k_l(F_3 s_3 - \beta_l\hat{k}_{t_3}) \\ \dot{\hat{m}}_1 = k_n(\Phi_3 s_3 - \beta_n\hat{m}_1) \\ \dot{\hat{\gamma}}_{d_3} = k_{d_3}(|s_3| - \beta_{d_3}\hat{\gamma}_{d_3}) \end{cases} \tag{40}$$

where $\hat{k}_{t_3}$ is the estimate of k_{t_3}, $\hat{m}_1$ is the estimate of m_1, $\hat{\gamma}_{d_3}$ is the estimate of γ_{d_1}, $k_i(i = 5, 6, l, n, d_3)$ and $\beta_j(j = l, n, d_3)$ are positive constant. δ_3 is the output of anti-windup saturation compensator designed as

$$\dot{\delta}_3 = -k_{c_6}\delta_3 + \Delta F_{\text{total}} \tag{41}$$

where k_{c_6} is a positive constant.

(2) *Relative attitude control design*

Define a sliding variable

$$\boldsymbol{s}_4 = \dot{\boldsymbol{\eta}} + k_7\boldsymbol{\eta} \tag{42}$$

From (6), (7), and parameter linearisation, we can derive

$$\begin{aligned} \boldsymbol{I}_1\frac{\mathrm{d}}{\mathrm{dt}}(\boldsymbol{R}_{r_1}^{-1}\boldsymbol{s}_4) &= \boldsymbol{I}_1(\boldsymbol{R}_{r_1}^{-1}\dot{\boldsymbol{s}}_4 + \dot{\boldsymbol{R}}_{r_1}^{-1}\boldsymbol{s}_4) \\ &= \boldsymbol{I}_1[\dot{\boldsymbol{R}}_{r_1}^{-1}(\dot{\boldsymbol{\eta}}+k_7\boldsymbol{\eta}) + \boldsymbol{R}_{r_1}^{-1}(\ddot{\boldsymbol{\eta}}+k_7\dot{\boldsymbol{\eta}})] \\ &= \boldsymbol{I}_1\dot{\Omega} + \boldsymbol{I}_1\dot{\boldsymbol{R}}_{r_1}^{-1}k_7\boldsymbol{\eta} + \boldsymbol{I}_1\boldsymbol{R}_{r_1}^{-1}k_7\dot{\boldsymbol{\eta}} \\ &= \boldsymbol{F}_2\boldsymbol{\epsilon} + \boldsymbol{\Phi}_4\boldsymbol{I}_m + \boldsymbol{\tau}_0 + \boldsymbol{d}_2 \end{aligned} \tag{43}$$

where $\boldsymbol{\Phi}_4 = -\boldsymbol{S}(\boldsymbol{\Omega}_1)L(\boldsymbol{\Omega}_1) + L(\dot{\boldsymbol{R}}_{r_1}^{-1}k_7\boldsymbol{\eta}) + L(\boldsymbol{R}_{r_1}^{-1}k_7\dot{\boldsymbol{\eta}}) - L(\dot{\boldsymbol{R}}_{r_{12}}\boldsymbol{\Omega}_2) - L(\boldsymbol{R}_{r_{12}}\dot{\boldsymbol{\Omega}}_2)$.

Design the relative attitude control input

$$\boldsymbol{\tau}_0 = -k_8\boldsymbol{R}_{r_1}^{-1}\boldsymbol{s}_4 + k_{c_7}\boldsymbol{\delta}_4 - \boldsymbol{\Phi}_4\hat{\boldsymbol{I}}_m - \boldsymbol{F}_2\hat{\boldsymbol{\epsilon}} - \boldsymbol{\gamma}_4 \tag{44}$$

$$\boldsymbol{\gamma}_4 = \begin{cases} \hat{\gamma}_{d_2}\dfrac{\boldsymbol{R}_{r_1}^{-1}\boldsymbol{s}_4}{\| \boldsymbol{R}_{r_1}^{-1}\boldsymbol{s}_4 \|} & \text{if } \hat{\gamma}_{d_2} \| \boldsymbol{R}_{r_1}^{-1}\boldsymbol{s}_4 \| > \kappa_4 \\ \hat{\gamma}_{d_2}^2\dfrac{\boldsymbol{R}_{r_1}^{-1}\boldsymbol{s}_4}{\kappa_4} & \text{if } \hat{\gamma}_{d_2} \| \boldsymbol{R}_{r_1}^{-1}\boldsymbol{s}_4 \| \le \kappa_4 \end{cases} \tag{45}$$

and the adaptation laws

$$\begin{cases} \dot{\hat{\boldsymbol{\epsilon}}} = k_a[\boldsymbol{F}_2^{\mathrm{T}}(\boldsymbol{R}_{r_1}^{-1}\boldsymbol{s}_4) - \beta_a\hat{\boldsymbol{\epsilon}}] \\ \dot{\hat{\boldsymbol{I}}}_m = k_b[\hat{\boldsymbol{\Phi}}_2^{\mathrm{T}}(\boldsymbol{R}_{r_1}^{-1}\boldsymbol{s}_4) - \beta_b\hat{\boldsymbol{I}}_m] \\ \dot{\hat{\gamma}}_{d_2} = k_{d_4}(\| \boldsymbol{R}_{r_1}^{-1}\boldsymbol{s}_4 \| - \beta_{d_4}\hat{\gamma}_{d_4}) \end{cases} \tag{46}$$

where $\hat{\gamma}_{d_2}$ is the estimate of γ_{d_2}, $k_i(i = 7, 8, a, b, d_4)$ and $\beta_j(j = a, b, d_4)$ are positive constant. $\boldsymbol{\delta}_4$ is the output of anti-windup saturation compensator designed as

$$\dot{\boldsymbol{\delta}}_4 = -k_{c_8}\boldsymbol{\delta}_4 + \Delta\boldsymbol{\tau} \tag{47}$$

where k_{c_8} is a positive constant.

Remark 9: It should be mentioned that the controlled variable here is relative attitude, which is different from the controlled variable of inner loop in RPC.

Theorem 2: For the relative motion of the quadrotor and vessel system (6) and (7) with input saturation (9) under Assumptions 1–4, the proposed RAC (38), (40), (44), and (46) can guarantee that all closed-loop signals converge to a small neighbourhood of zero.

Proof: Define the estimate errors $\tilde{k}_{t_3} = \hat{k}_{t_3} - k_{t_3}$, $\tilde{m}_1 = \hat{m}_1 - m_1$, $\tilde{\gamma}_{d_3} = \hat{\gamma}_{d_3} - \gamma_{d_3}$, $\tilde{\gamma}_{d_2} = \hat{\gamma}_{d_2} - \gamma_{d_2}$, respectively.

Considering the Lyapunov function candidate as

$$V_n = V_a + V_b \tag{48}$$

where

$$V_a = \frac{1}{2}m_1 s_3^2 + \frac{1}{2}\delta_3^2 + \frac{1}{2k_l}\tilde{k}_{t_3}^2 + \frac{1}{2k_n}\tilde{m}_1^2 + \frac{1}{2k_{d_3}}\tilde{\gamma}_{d_3}^2$$

$$\begin{aligned} V_b = &\frac{1}{2}(\boldsymbol{R}_{r_1}^{-1}\boldsymbol{s}_4)^{\mathrm{T}}\boldsymbol{I}_1(\boldsymbol{R}_{r_1}^{-1}\boldsymbol{s}_4) + \frac{1}{2}\boldsymbol{\delta}_4^{\mathrm{T}}\boldsymbol{\delta}_4 + \frac{1}{2k_a}\tilde{\boldsymbol{\epsilon}}^{\mathrm{T}}\tilde{\boldsymbol{\epsilon}} \\ &+\frac{1}{2k_b}\tilde{\boldsymbol{I}}_m^{\mathrm{T}}\tilde{\boldsymbol{I}}_m + \frac{1}{2k_{d_4}}\tilde{\gamma}_{d_2}^2 \end{aligned}$$

Differentiating (29) with respect to time yields

$$\begin{aligned} \dot{V}_n = &m_1 s_3\dot{s}_3 + \frac{1}{k_l}\tilde{k}_{t_3}\dot{\tilde{k}}_{t_3} + \frac{1}{k_n}\tilde{m}_1\dot{\tilde{m}}_1 + \frac{1}{k_{d_3}}\tilde{\gamma}_{d_3}\dot{\tilde{\gamma}}_{d_3} \\ &+\delta_3\dot{\delta}_3 + (\boldsymbol{R}_{r_1}^{-1}\boldsymbol{s}_4)^{\mathrm{T}}\boldsymbol{I}_1\frac{d}{dt}(\boldsymbol{R}_{r_1}^{-1}\boldsymbol{s}_4) + \frac{1}{k_a}\tilde{\boldsymbol{\epsilon}}^{\mathrm{T}}\dot{\tilde{\boldsymbol{\epsilon}}} \\ &+\frac{1}{k_b}\tilde{\boldsymbol{I}}_m^{\mathrm{T}}\dot{\tilde{\boldsymbol{I}}}_m + \frac{1}{k_{d_4}}\tilde{\gamma}_{d_2}\dot{\tilde{\gamma}}_{d_2} + \boldsymbol{\delta}_4^T\dot{\boldsymbol{\delta}}_4 \end{aligned} \tag{49}$$

With (37), (38), (43), and (44), (49) can be derived as

$$\begin{aligned} \dot{V}_n = &-k_6 s_3^2 + k_{c_5}s_3\delta_3 - s_3\Phi_3\tilde{m}_1 - s_3F_3\tilde{k}_{t_3} + s_3 d_3 \\ &-s_3\gamma_3 + \frac{1}{k_l}\tilde{k}_{t_3}\dot{\tilde{k}}_{t_3} + \frac{1}{k_n}\tilde{m}_1\dot{\tilde{m}}_1 + \frac{1}{k_{d_3}}\tilde{\gamma}_{d_3}\dot{\tilde{\gamma}}_{d_3} \\ &-k_{c_6}\delta_3^2 + \delta_3\Delta F_{\text{total}} - k_8(\boldsymbol{R}_{r_1}^{-1}\boldsymbol{s}_4)^{\mathrm{T}}(\boldsymbol{R}_{r_1}^{-1}\boldsymbol{s}_4) \\ &+k_{c_7}(\boldsymbol{R}_{r_1}^{-1}\boldsymbol{s}_4)^{\mathrm{T}}\boldsymbol{\delta}_4 - (\boldsymbol{R}_{r_1}^{-1}\boldsymbol{s}_4)^{\mathrm{T}}\boldsymbol{F}_4\tilde{\boldsymbol{\epsilon}} + \frac{1}{k_a}\tilde{\boldsymbol{\epsilon}}^{\mathrm{T}}\dot{\tilde{\boldsymbol{\epsilon}}} \\ &+(\boldsymbol{R}_{r_1}^{-1}\boldsymbol{s}_4)^{\mathrm{T}}\boldsymbol{d}_2 - (\boldsymbol{R}_{r_1}^{-1}\boldsymbol{s}_4)^{\mathrm{T}}\boldsymbol{\gamma}_4 - (\boldsymbol{R}_{r_1}^{-1}\boldsymbol{s}_4)^{\mathrm{T}}\hat{\boldsymbol{\Phi}}_4\tilde{\boldsymbol{I}}_m \\ &+\frac{1}{k_b}\tilde{\boldsymbol{I}}_m^{\mathrm{T}}\dot{\tilde{\boldsymbol{I}}}_m + \frac{1}{k_{d_4}}\tilde{\gamma}_{d_2}\dot{\tilde{\gamma}}_{d_2} - k_{c_8}\boldsymbol{\delta}_4^{\mathrm{T}}\boldsymbol{\delta}_4 + \boldsymbol{\delta}_4^{\mathrm{T}}\Delta\boldsymbol{\tau} \end{aligned} \tag{50}$$

Noticing $s_3 d_3 \le \gamma_{d_3}|s_3|$ and $(\boldsymbol{R}_{r_1}^{-1}\boldsymbol{s}_4)^{\mathrm{T}}\boldsymbol{d}_2 \le \gamma_{d_2} \| \boldsymbol{R}_{r_1}^{-1}\boldsymbol{s}_4 \|$ and substituting adaptation laws (40) and (46) to (50), we have

$$\begin{aligned}\dot{V}_n \le & -\left(k_6-\frac{k_{c_5}}{2}\right)|s_3|^2-\frac{2k_{c_6}-k_{c_5}-1}{2}|\delta_3|^2-\frac{\beta_l}{2}\|\tilde{k}_{t_3}\|^2\\ & -\frac{\beta_n}{2}|\tilde{m}_1|^2-\frac{\beta_{d_3}}{2}|\tilde{\gamma}_{d_3}|^2-\left(k_8-\frac{k_{c_7}}{2}\right)\|\boldsymbol{R}_{r_1}^{-1}\boldsymbol{s}_4\|^2\\ & -\frac{2k_{c_8}-k_{c_7}-1}{2}\|\boldsymbol{\delta}_4\|^2-\frac{\beta_a}{2}\|\tilde{\boldsymbol{\epsilon}}\|^2-\frac{\beta_b}{2}\|\tilde{\boldsymbol{I}}_m\|^2\\ & -\frac{\beta_{d_4}}{2}|\tilde{\gamma}_{d_2}|^2+\iota_2^*\end{aligned} \tag{51}$$

where

$$\begin{aligned}\iota_2^* = & \frac{\beta_l}{2}|k_{t_3}|^2+\frac{\beta_n}{2}|m_1|^2+\frac{\beta_{d_3}}{2}|\gamma_{d_3}|^2+\frac{\beta_a}{2}\|\boldsymbol{\epsilon}\|^2\\ & +\frac{\beta_b}{2}\|\boldsymbol{I}_m\|^2+\frac{\beta_{d_4}}{2}|\gamma_{d_2}|^2+\frac{1}{2}|\Delta F_{\text{total}}|^2\\ & +\frac{1}{2}\|\Delta\boldsymbol{\tau}\|^2+\frac{\kappa_3}{4}+\frac{\kappa_4}{4}.\end{aligned}$$

If $2k_6 > k_{c_5}$, $2k_8 > k_{c_7}$, $2k_{c_6} > k_{c_5}+1$, and $2k_{c_8} > k_{c_7}+1$, then $\dot{V}_m \le -\rho_2 V_m + \iota_2^*$, where

$$\begin{aligned}\rho_2 = & \frac{\rho_0^*}{\rho_{\max}^*},\\ \rho_0^* = & \min\left(k_6-\frac{k_{c_5}}{2},\frac{2k_{c_6}-k_{c_5}-1}{2},\frac{\beta_l}{2},\frac{\beta_n}{2},\frac{\beta_{d_3}}{2},\right.\\ & \left.k_8-\frac{k_{c_7}}{2},\frac{2k_{c_8}-k_{c_7}-1}{2},\frac{\beta_a}{2},\frac{\beta_b}{2},\frac{\beta_{d_4}}{2}\right),\\ \rho_{\max}^* = & \frac{1}{2}\max\left(m_1,1,\frac{1}{k_l},\frac{1}{k_n},\frac{1}{k_{d_3}},\lambda_{\max}(\boldsymbol{I}_1),\frac{1}{k_a},\frac{1}{k_b},\frac{1}{k_{d_4}}\right).\end{aligned}$$

Then, applying comparison principle, we derive

$$V_n(t) \le \left(V_n(0)-\frac{\iota_2^*}{\rho_2}\right)e^{-\rho_2 t}+\frac{\iota_2^*}{\rho_2} \le \frac{\iota_2^*}{\rho_2}.$$

It implies that s_3, $\boldsymbol{s}_4$, $\tilde{k}_{t_3}$, $\tilde{m}_1$, $\tilde{\boldsymbol{\epsilon}}$, $\tilde{\boldsymbol{I}}_m$, $\tilde{\gamma}_{d_3}$, $\tilde{\gamma}_{d_2}$, δ_3, $\boldsymbol{\delta}_4$ are coverage eventually to a small set. Then, from (36) and (42), we can conclude z and $\boldsymbol{\eta}$ are coverage to a small neighbourhood of zero. Besides, From (7), (38), and (44), we can conclude that all states of the closed-loop are bounded. □

5 Simulations

To verify the effectiveness of the proposed RPC and RAC, a sequence of numerical simulations are presented. The model parameters of quadrotor and vessel are shown in Table 1 [31]. Some of the sample values of pitch, heave, and roll motions coefficients ζ_i and ϱ_i in different sea state are listed in Table 2 [18].

Wind model is established in consideration of the three main components: steady wind, atmospheric turbulence, and gusts. The equivalent turbulence can be obtained using a shaping filter with white noise input. The transfer functions of the shaping filter are [18]

$$\begin{aligned}T_x(s) = & \sigma_x\sqrt{q_x}\frac{1.258s+5.033q_x}{s^2+6.829q_xs+5.033q_x^2},\\ T_j(s) = & \sigma_j\sqrt{q_j}\frac{2.208s^2+17.855q_js+6.498q_j^2}{s^3+12.836q_js^2+6.498q_j^3},\end{aligned}$$

where $j = y, z$, $\sigma_i (i = x, y, z)$ is the turbulence intensity, $q_i = V_{\text{wind}}/L_i$, V_{wind} is vertical component of trimmed speed, L_i is the turbulence length scale. The model can be extended to rotational velocity components in the same form. Steady wind and gusts are depicted by the combination of constant and cosine function model

Table 1 Model parameters for quadrotor and vessel

Parameter	Value	Parameter	Value
m_1	2 kg	m_{11}	150 kg
I_x	1.2416 Nm.s^2/rad	m_{22}	150 kg
I_y	1.2416 Nm.s^2/rad	m_{33}	100 kg.m^2
I_z	2.4832 Nm.s^2/rad	d_{11}	150 kg/s
K_{t_1}	0.01 N.s/m	d_{22}	150 kg/s
K_{t_2}	0.01 N.s/m	d_{33}	100 kg.m^2/s
K_{t_3}	0.01 N.s/m	T_x	100 N
K_{r_1}	0.001 Nm.s/rad	T_y	−50 N
K_{r_2}	0.001 Nm.s/rad	T_z	0 Nm
K_{r_3}	0.001 Nm.s/rad		

Table 2 Sample amplitudes and frequencies

Sea state	2	6
pitch amplitude, deg	0.399	4.791
heave amplitude, m	0.137	1.652
roll amplitude, deg	0.216	2.59
pitch frequency, Hz	0.086	0.086
heave frequency, Hz	0.082	0.082
roll frequency, Hz	0.114	0.114

$$\begin{bmatrix}W_x\\W_y\\W_z\end{bmatrix}=\begin{bmatrix}W_\phi\\W_\theta\\W_\psi\end{bmatrix}=\begin{bmatrix}0.5-0.04\cos(0.5t)\\0.5+0.05\cos(0.5t)\\0.5-0.03\cos(0.5t)\end{bmatrix}.$$

The magnitude of the quadrotor's actuated control inputs are specified in the range of $F_{\text{total}} \in [-25, 25]$ N, $\tau_x, \tau_y, \tau_z \in [-25, 25]$ Nm.

5.1 Simulations of RPC

The simulation of RPC is performed in sea state 2. The desired relative position and desired yaw of the quadrotor are set as $\boldsymbol{\xi}_d = [0, 0, 0.5]$ m and $\psi_{1d} = \pi/8$, respectively. The initial conditions of the quadrotor and vessel are selected as $\boldsymbol{\xi}_1(0) = [6, 6, 5]^{\mathrm{T}}$ m, $\boldsymbol{V}_1(0) = [0.1, 0.1, 0.1]^{\mathrm{T}}$ m/s, $\boldsymbol{\eta}_1(0) = [0, 0, 0]^T$ rad, $\boldsymbol{\Omega}_1(0) = [0.1, 0.1, 0.1]^T$ rad/s, $\boldsymbol{\xi}_2(0) = [1, 1, 0]^{\mathrm{T}}$ m, $\boldsymbol{\eta}_2(0) = [0, 0, 0]^{\mathrm{T}}$ rad, $\boldsymbol{V}_2(0) = [0, 0, 0]^{\mathrm{T}}$ m/s, $\boldsymbol{\Omega}_2(0) = [0, 0, 0]^T$ rad/s. The initial estimate values of the quadrotor are set as $\hat{\boldsymbol{\sigma}}(0) = [0.05, 0.05, 0.05]^{\mathrm{T}}$ N.s/m, $\hat{m}_1(0) = 2.2$ kg, $\hat{\boldsymbol{\epsilon}}(0) = [0, 0, 0]^{\mathrm{T}}$ N.s/rad, $\hat{\boldsymbol{I}}_m(0) = [1, 1, 2]^{\mathrm{T}}$ Nm.s^2/rad), $\hat{\gamma}_{d_1}(0) = 0$, $\hat{\gamma}_{d_2}^*(0) = 0$. The wind disturbances' parameters are set as $\sigma_i = 2 (i = x, y, z, \phi, \theta, \psi)$, $L_x = L_z = L_\phi = L_\psi = 23$ m, $L_\theta = L_y = 3$ m, $V_{wind} = 10$ m/s. The external disturbances of vessel are given as $\boldsymbol{d}_t = 0.2\sin(0.5t) + 0.2\sin(0.6t) \times [1, 1, 1]^{\mathrm{T}}$ N, $\boldsymbol{d}_s = 0.05\sin(0.5t) + 0.05\sin(0.6t) \times [1, 1, 1]^{\mathrm{T}}$ Nm. The control parameters are chosen as $k_1 = 0.3, k_2 = 4.5$, $k_3 = 1.5, k_4 = 95$, $k_{c_1} = 3, k_{c_2} = 15, k_{c_3} = 20$, $k_{c_4} = 25, k_\sigma = 0.3$, $k_m = 0.04, k_{d_1} = 0.2$, $k_\epsilon = 0.5, k_I = 1.3, k_{d_2} = 0.5, \beta_\sigma = 1, \beta_\epsilon = 0.5, \beta_m = 0.2, \beta_i = 0.5$, $\beta_{d_1} = 0.2, \beta_{d_2} = 0.5, \kappa_1 = 0.015, \kappa_2 = 0.02, \omega_n = 25, \Lambda = 1.5$.

The simulation results of RPC are shown in Figs. 3–5. Fig. 3 shows the quadrotor can accomplish the approaching phase under the control of RPC, that is, the quadrotor can track the trajectory in Oxy plane of the vessel and maintains at 0.5 m right above the vessel. Fig. 4 (top left) demonstrates that the relative position in Oxy plane and relative altitude coverage to zero and 0.5 within 15(s), respectively. The attitude of the quadrotor shown in Fig. 4 (top right) illustrates that the actual attitude is synchronised with the desired attitude of the quadrotor. The attitude synchronisation is achieved within 3(s) indicating that the inner control loop can be quickly stabilised. Fig. 4 (bottom left) describes the relative velocity and angular velocity of quadrotor. Fig. 4 (bottom right)

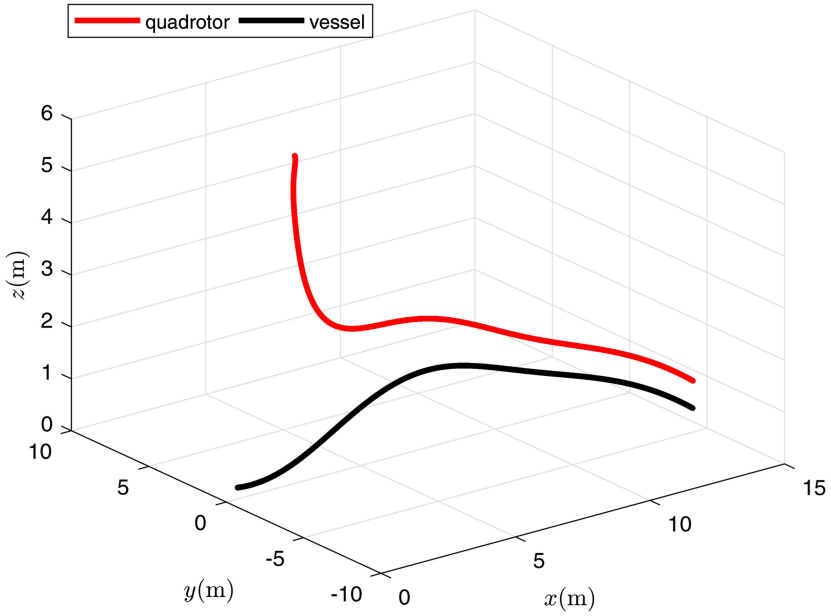

Fig. 3 *Trajectories of quadrotor and vessel in RPC*

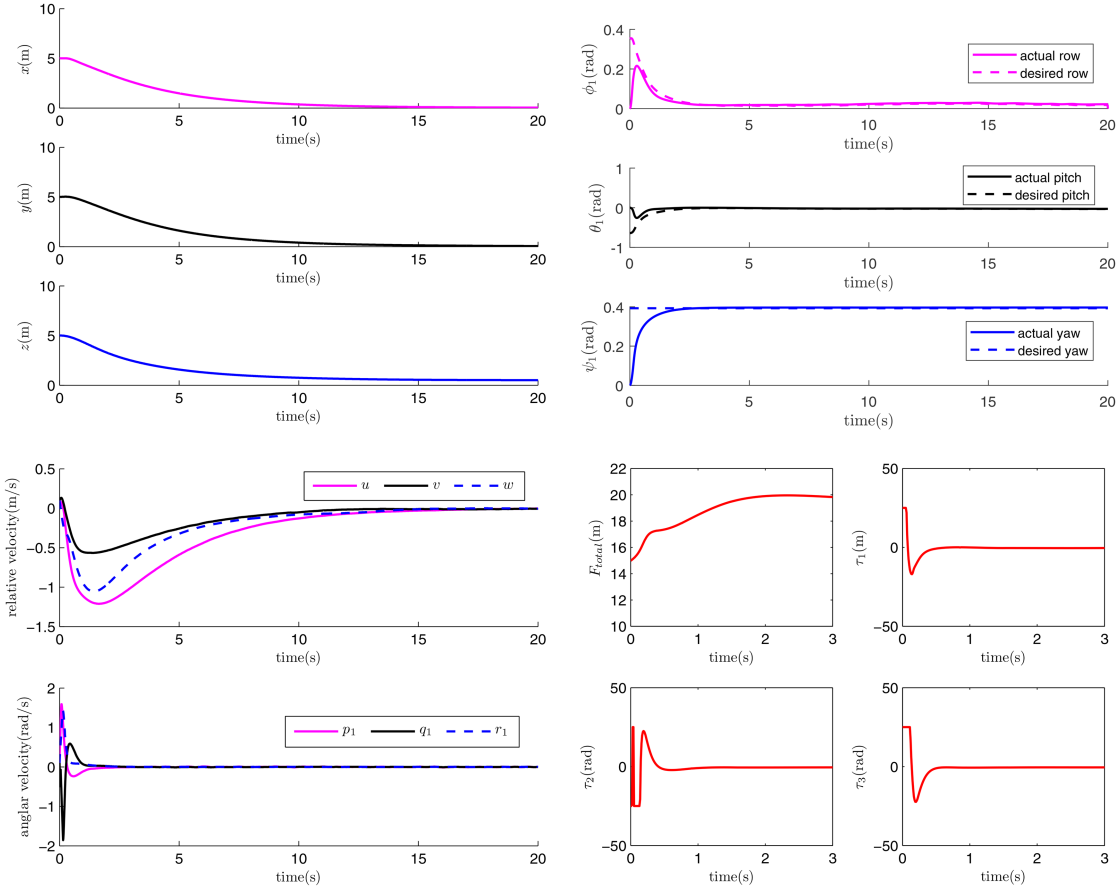

Fig. 4 *Relative position (top left), relative velocity, and anglar velocity of quadrotor (bottom left), attitude of quadrotor (top right), and control inputs of quadrotor (bottom right) in RPC*

describes the control inputs. It can be seen that control inputs with input constraints are limited before putting them on the actual actuators. Fig. 5 (top left) describes the wind disturbances. Fig. 5 (top right and bottom left) describe the inertial parameter estimations. Fig. 5 (bottom right) describes the estimations of disturbances' bounds. It is implied that all estimation signals are well adapted to the dynamics with bounded uncertainties.

5.2 Simulations of RAC

The initial conditions of the quadrotor and vessel in RAC are set as follows corresponding to the final conditions in RPC. $\boldsymbol{\xi}_1(0) = [14.18, -5.52, 1.09]^{\mathrm{T}}$ m, $\boldsymbol{\eta}_1(0) = [0.02, -0.03, 0.39]^{\mathrm{T}}$ rad, $\boldsymbol{V}_1(0) = [0.46, -0.58, -0.3]^{\mathrm{T}}$ m/s, $\boldsymbol{\Omega}_1(0) = [0, 0, 0]^{\mathrm{T}}$ rad/s, $\boldsymbol{\xi}_2(0) = [14.18, -5.52, 0.59]^{\mathrm{T}}$ m, $\boldsymbol{\eta}_2(0) = [0.42, 0.67, 0.13]^{\mathrm{T}}$ rad, $\boldsymbol{V}_2(0) = [0.46, -0.58, -0.3]^{\mathrm{T}}$ m/s, $\boldsymbol{\Omega}_2(0) = [0, 0, 0]^{\mathrm{T}}$ rad/s. The initial estimate values of the quadrotor in RAC are the same as RPC. The

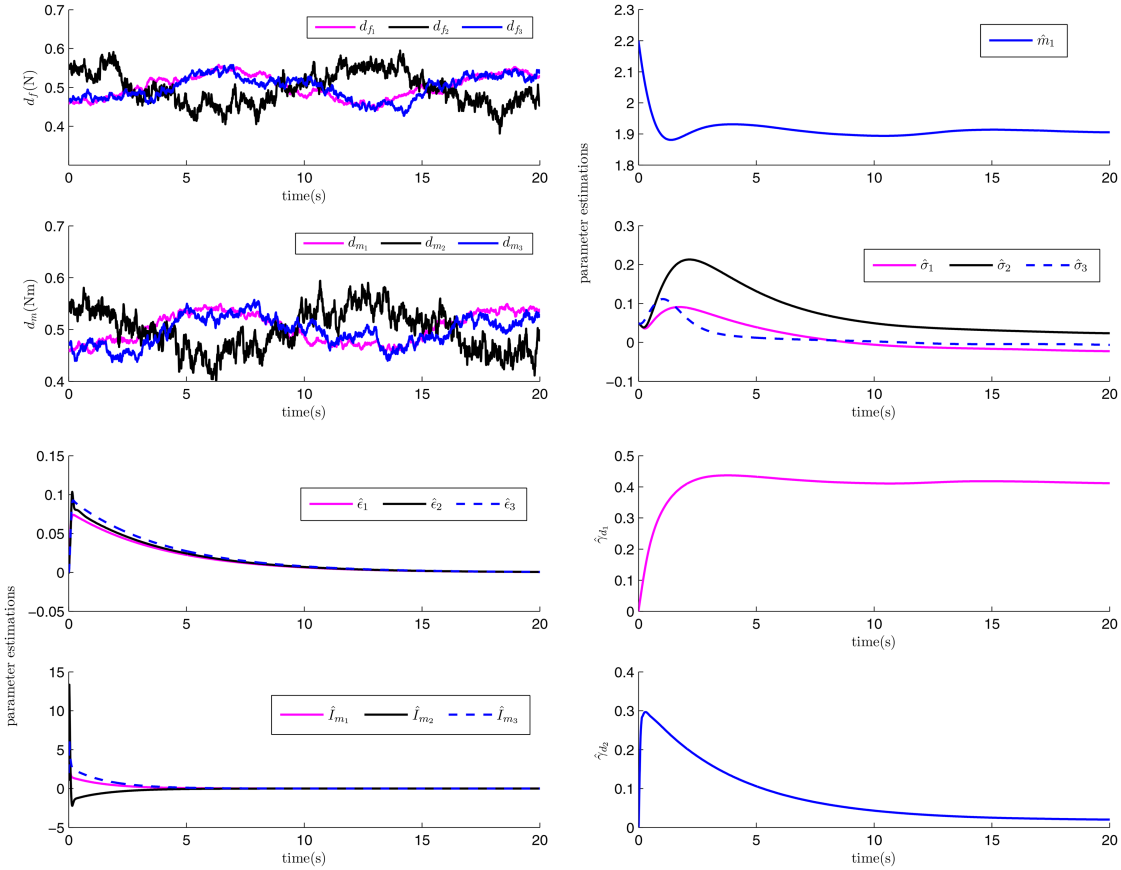

Fig. 5 *Wind disturbances (top left), inertial parameter estimations (top right and bottom left), and estimations of disturbances' bounds (bottom right) in RPC*

control parameters are set as $k_5 = 5, k_6 = 25,\ k_7 = 5, k_8 = 35,\ k_{c_5} = 3, k_{c_6} = 15, k_{c_7} = 20, k_{c_8} = 25, k_l = 0.08, k_n = 0.1, k_{d_3} = 0.11,\ k_a = 0.5,\ k_b = 0.2, k_{d_4} = 0.8,\ \beta_l = 0.1, \beta_n = 0.1,\ \beta_{d_3} = 0.2, \beta_a = 0.1,\ \beta_b = 0.2, \beta_{d_4} = 0.1, \kappa_3 = 0.015, \kappa_4 = 0.02.$

As for wind disturbances, we demonstrate two typical wind conditions in Fig. 6. Wind condition 1 (top left figure in Fig. 6) denotes that the steady wind disturbance is 0.5 N and turbulence intensity $\sigma_i = 8(i = x, y, z, \phi, \theta, \psi)$, while wind condition 2 (top right figure in Fig. 6) represents that the steady wind disturbance is $1(N)$ and turbulence intensity $\sigma_i = 15(i = x, y, z, \phi, \theta, \psi)$. The other wind parameters in these two conditions are the same as RPC.

A series of figures similar to the RPC simulation are shown in Figs. 6–8. To decline the tracking errors in *Oxy* plane which are out of the control of RAC, the control speed should be as rapid as possible. As demonstrated in Fig. 7 (top right and bottom left), the relative altitude and relative attitude of quadrotor and vessel coverage to zero within 1 s, the tracking errors in *Oxy* plane are $x = -0.12$ m and $y = -0.09$ m satisfying the requirement of landing phase. Fig. 7 (bottom right) describes the control inputs with input constraints are limited before putting them on the actual actuators. Additionally, Fig. 6 (bottom left and bottom right) and Fig. 8 (top left) illustrate all estimation signals including inertial parameter estimations and estimations of disturbances' bounds are bounded.

To verify robustness of RAC, plenty of reduplicative simulations are presented under different wind conditions and sea states. The landing point statistical results in *Oxy* plane are given in Fig. 8 (top right, bottom left, and bottom right), where the red cycle represents the landing point requirement boundary $R = 0.45$ m, the green cycle is the available landing point boundary $R = 0.2$ m under the control of RAC at wind condition 1 and sea state 2. Multiple stochastic simulation results show that the tracking errors in *Oxy* plane remain within the required range under different disturbances, and the control performance decreases when wind or wave intension enhance. Additionally, to illustrate the effectiveness and the robustness of the proposed method (PM) to the perturbation more persuasively, the comparison simulation is carried out shown in Fig. 8 (top right), where blue cross-shaped points represent the landing points under the PM, pink starlike points represent the landing points under the PM without disturbance adaptive estimation (WDAE). It can be seen obviously that the landing points errors remain within 0.2 m under PM, while the landing points errors enhance dramatically under WDAE. So we can claim that the PM provides a better robustness to the perturbation.

Thus, the proposed control strategy shows its effectiveness and robustness to successfully accomplish the task for a quadrotor landing on a vessel.

6 Conclusions

In this paper, we devote to solving the autonomous vessel landing problem for a quadrotor considering input saturation, parameter uncertainty, and external disturbances. A non-linear underactuated 6-DOF relative motion model with four control inputs is established. To address the model properties of underactuated and strongly coupled, the vessel landing is divided to two phases which correspond to controllers RPC and RAC. The RAC and RPC are both designed in the framework of adaptive algorithm based on sliding mode control technique to estimate and compensate the control input saturation effect and model uncertainties. Stability analysis implies that the closed-loop sysytems are uniformly ultimately bounded. The effectiveness of the proposed control approach is verified by simulations.

7 Acknowledgments

This work was supported by the National Natural Science Foundation of China (grant nos. 61503010 and 61703018), the Aeronautical Science Foundation of China (grant no. 2016ZA51001), the China Postdoctoral Science Foundation (No. 2017T100024), and the Fundamental Research Funds for the Central Universities (grant nos. YWF-17-BJ-Y-143 and YWF-18-BJ-Y-108).

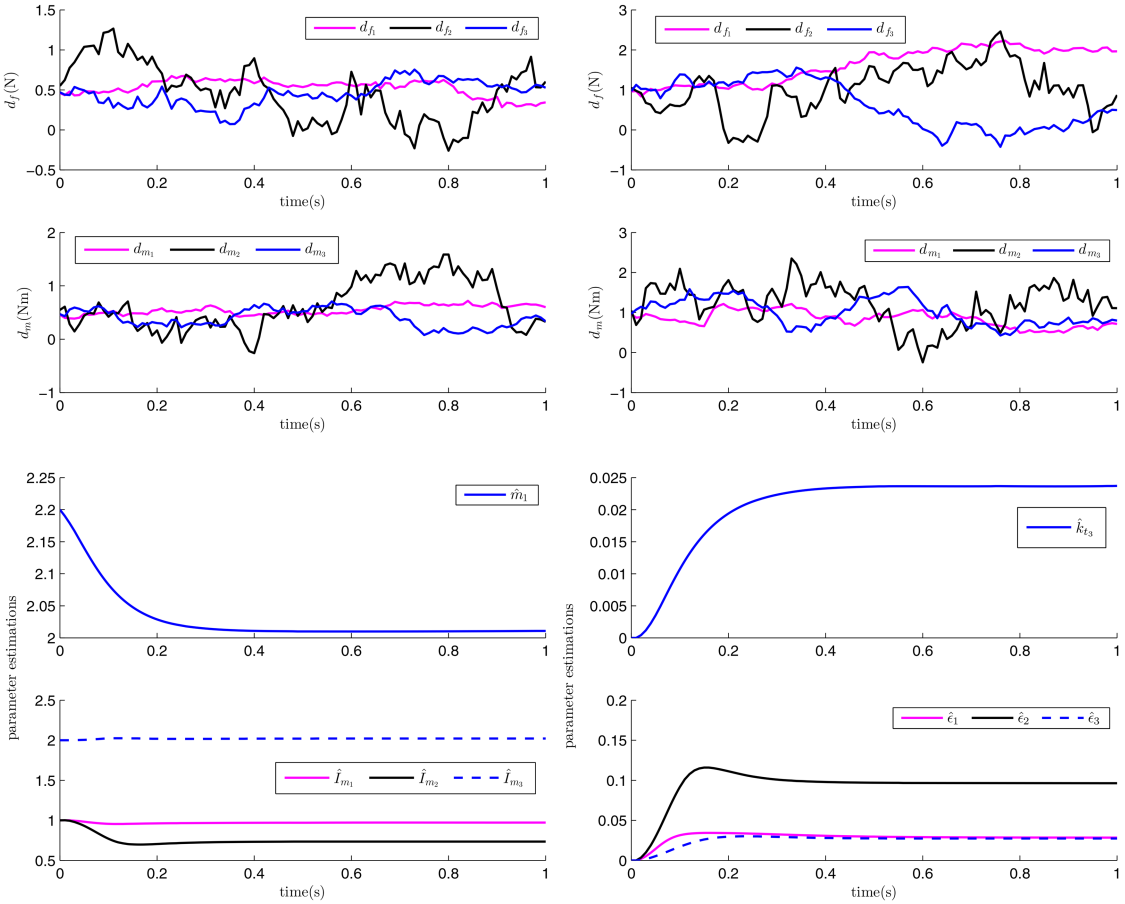

Fig. 6 *Wind disturbances (top left and top right) and inertial parameter estimations (bottom left and bottom right) in RAC*

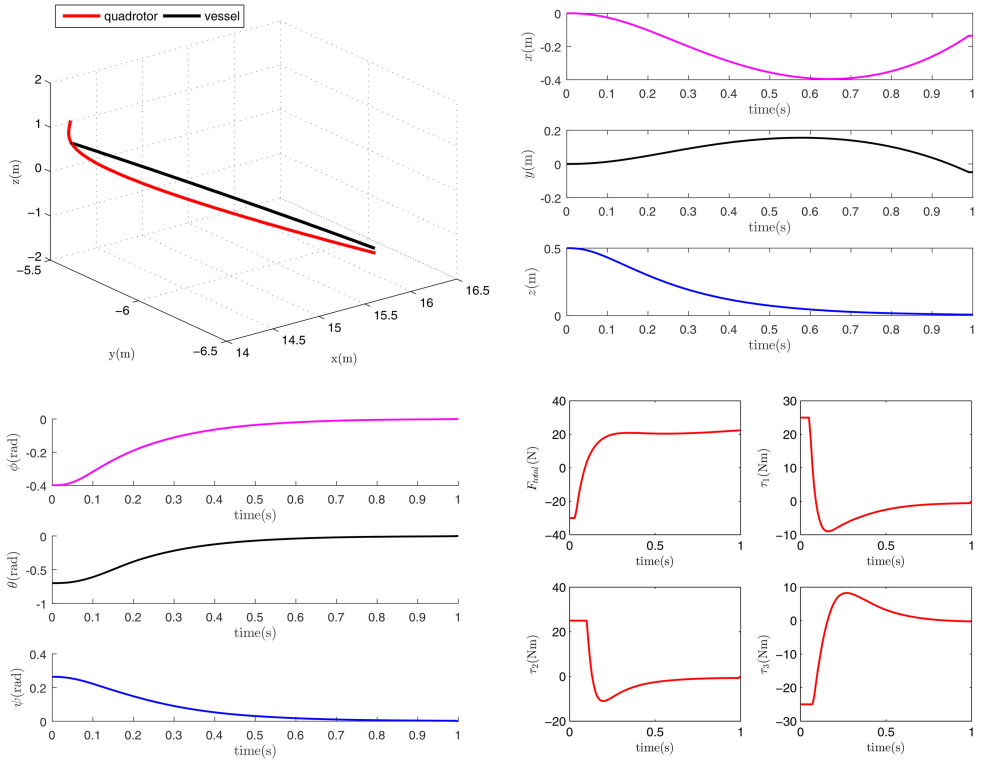

Fig. 7 *Trajectories of quadrotor and vessel (top left), relative position (top right), relative attitude (bottom left), and control inputs of quadrotor (bottom right) in RAC*

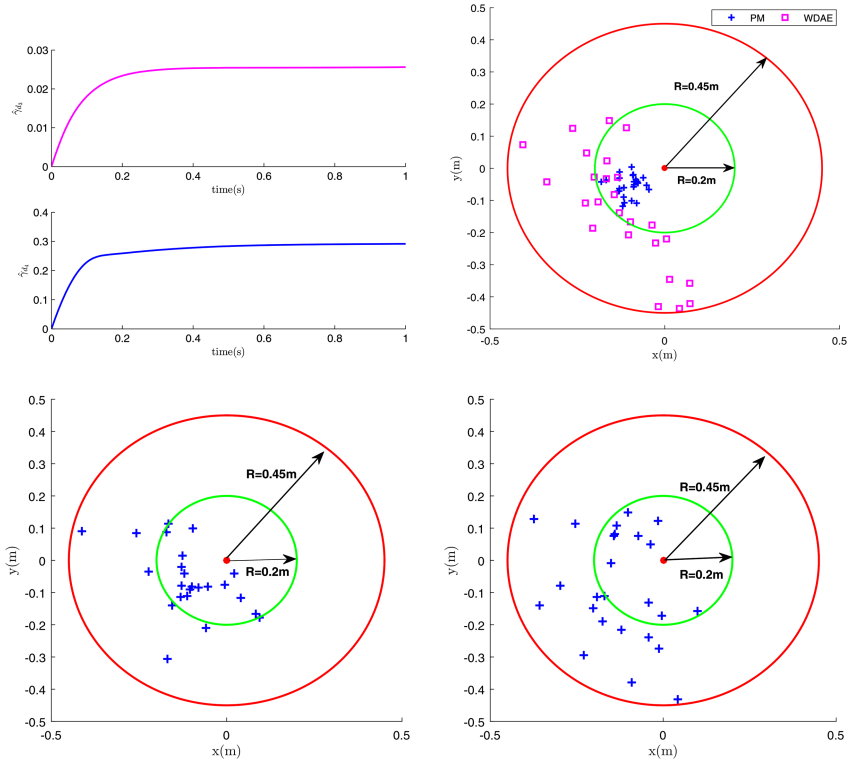

Fig. 8 *Estimations of disturbances' bounds in RAC (top left), landing points at wind condition 1 and sea state 2 (top right), landing points at wind condition 2 and sea state 2 (bottom left), and landing points at wind condition 1 and sea state 6 (bottom right)*

8 References

[1] Zuo, Z., Ru, P.: 'Augmented L_1 adaptive tracking control of quadrotor unmanned aircrafts', *IEEE Trans. Aerosp. Electron. Syst.*, 2014, **50**, (4), pp. 3090–3101

[2] Islam, S., Liu, P.X., Saddik, A.E.: 'Robust control of four-rotor unmanned aerial vehicle with disturbance uncertainty', *IEEE Trans. Ind. Electron.*, 2015, **62**, (3), pp. 1563–1571

[3] Xiong, J., Zheng, E.: 'Position and attitude tracking control for a quadrotor UAV', *ISA Trans.*, 2014, **53**, pp. 725–731

[4] Tan, C.K., Wang, J., Paw, Y.C., *et al.*: 'Autonomous ship deck landing of a quadrotor using invariant ellipsoid method', *IEEE Trans. Aerosp. Electron. Syst.*, 2016, **52**, (2), pp. 891–903

[5] Shin, H., You, D., Shim, D.H.: 'Autonomous shipboard landing algorithm for unmanned helicopters in crosswind', *J. Intell. Robot. Syst.*, 2014, **74**, pp. 347–361

[6] Zheng, Z., Jin, Z., Sun, L., *et al.*: 'Adaptive sliding mode relative motion control for autonomous carrier landing of fixed-wing unmanned aerial vehicles', *IEEE Access*, 2017, **5**, pp. 5556–5565

[7] Liu, Z., Wang, Y., Hao, X.: 'Coordinated landing control of unmanned aerial vehicle'. Int. Conf. on Electronics, Communications and Control, Ningbo, China, 2011, pp. 1965–1970

[8] Li, J., Duan, H.: 'Simplified brain storm optimization approach to control parameter optimization in F/A-18 automatic carrier landing system', *Aerosp. Sci. Technol.*, 2015, **42**, pp. 187–195

[9] Ma, Z., Hu, T., Shen, L.: 'Stereo vision guiding for the autonomous landing of fixed-wing UAVs: a saliency-inspired approach', *Int. J. Adv. Robot. Syst.*, 2016, **13**, Artical No. 43, pp. 1–13

[10] Saripalli, S.: 'Vision-based autonomous landing of an helicopter on a moving target'. AIAA Guidance Navigation, and Control Conf., Chicago, Illinois, USA, 2009, pp. 10–13

[11] Yu, Y., Wang, H., Li, N., *et al.*: 'Automatic carrier landing system based on active disturbance rejection control with a novel parameters optimizer', *Aerosp. Sci. Technol.*, 2017, **69**, pp. 149–160

[12] Deng, Y., Duan, H.: 'Control parameter design for automatic carrier landing system via pigeon-inspired optimization', *Nonlinear Dyn.*, 2016, **85**, (1), pp. 97–106

[13] Sun, L., Huo, W.: 'Robust adaptive relative position tracking and attitude synchronization for spacecraft rendezvous', *Aerosp. Sci. Technol.*, 2015, **41**, pp. 28–35

[14] Zhang, J., Zhao, S., Yang, Y.: 'Characteristic analysis for elliptical orbit hovering based on relative dynamics', *IEEE Trans. Aerosp. Electron. Syst.*, 2013, **49**, (4), pp. 2742–2750

[15] Zhang, J., Zhao, S., Zhang, Y.: 'Autonomous guidance for rendezvous phasing based on special-point-based maneuvers', *J. Guid. Control Dyn.*, 2014, **38**, (4), pp. 1–9

[16] Oh, S.R., Pathak, K., Agrawal, S.K., *et al.*: 'Approaches for a tether-guided landing of an autonomous helicopter', *IEEE Trans. Robot.*, 2006, **22**, (3), pp. 536–544

[17] Bodson, M., Athans, M.: 'Multivariable control of VTOL aircraft for shipboard landing'. AIAA Guidance Navigation, and Control Conf., Cincinnati, Ohio, USA, 1985, pp. 473–481

[18] Khantsis, S.: 'Control system design using evolutionary algorithms for autonomous shipboard recovery of unmanned aerial vehicles'. PhD Thesis, Royal Melbourne Institute of Technology, 2006

[19] Dong, W., Guo, Y.: 'Nonlinear tracking control of underactuated surface vessel', American Control Conf., Portland, Oregon, USA, 2005, pp. 4351–4356

[20] Azinheira, J.R., Moutinho, A.: 'Hover control of an uav with backstepping design including input saturations', *IEEE Trans. Control Syst. Technol.*, 2008, **16**, (3), pp. 517–526

[21] Zheng, Z., Huang, Y., Xie, L., *et al.*: 'Adaptive trajectory tracking control of a fully actuated surface vessel with asymmetrically constrained input and output', *IEEE Trans. Control Syst. Technol.*, doi: 10.1109/TCST.2017.2728518

[22] Cao, N., Lynch, A.F.: 'Inner-outer loop control for quadrotor uavs with input and state constraints', *IEEE Trans. Control Syst. Technol.*, 2016, **24**, (5), pp. 1797–1804

[23] Sun, L., Zheng, Z.: 'Disturbance observer-based robust backstepping attitude stabilization of spacecraft under input saturation and measurement uncertainty', *IEEE Trans. Ind. Electron.*, 2017, **64**, (10), pp. 7994–8002

[24] Sun, L., Zheng, Z.: 'Disturbance observer-based robust saturated control for spacecraft proximity maneuvers', *IEEE Trans. Control Syst. Technol.*, 2018, **26**, (2), pp. 684–692

[25] Zheng, Z., Sun, L., Xie, L.: 'Error constrained LOS path following of a surface vessel with actuator saturation and faults', *IEEE Trans. Syst. Man Cybern., Syst.*, doi: 10.1109/TSMC.2017.2717850

[26] Zheng, Z., Feroskhan, M.: 'Path following of a surface vessel with prescribed performance in the presence of input saturation and external disturbances', *IEEE/ASME Trans. Mech.*, 2017, **22**, (6), pp. 2564–2575

[27] Shtessel, Y., Buffington, J., Banda, S.: 'Multiple time scale flight control using re-configurable sliding modes', *AIAA J. Guid. Control Dyn.*, 1999, **22**, (6), pp. 873–883

[28] Shtessel, Y., Buffington, J., Banda, S.: 'Tailless aircraft flight control using multiple time scale re- configurable sliding modes', *IEEE Trans. Control Syst. Technol.*, 2002, **10**, (2), pp. 288–296

[29] Jin, C., Zhu, M., Sun, L., *et al.*: 'Relative motion modeling and control for a quadrotor landing on an unmanned vessel'. AIAA Guidance, Navigation, and Control Conf., Grapevine, Texas, USA, 2017

[30] Ghommam, J., Saad, M.: 'Autonomous landing of a quadrotor on a moving platform', *IEEE Trans. Aerosp. Electron. Syst.*, 2017, **53**, (3), pp. 1504–1519

[31] Madani, T., Benallegue, A.: 'Backstepping control for a quadrotor helicopter', IEEE/RSJ Int. Conf. Intell. Robots Syst., Beijing, China, 2006, pp. 3255–3260

[32] Pérez, T., Blanke, M. 'Mathematical ship modeling for control applications'. Technical Report, 2002

[33] Zuo, Z.: 'Trajectory tracking control design with command-filtered compensation for a quadrotor', *IET Control Theory Applic.*, 2010, **19**, (11), pp. 2343–2355

[34] Farrell, J., Sharma, M., Polycarpou, M.: 'Backstepping-based flight control with adaptive function approximation', *J. Guid. Control Dyn.*, 2012, **28**, (6), pp. 1089–1102
[35] Sun, L., Zuo, Z.: 'Nonlinear adaptive trajectory tracking control for a quadrotor with parametric uncertainty', *Proc. Inst. Mech. Eng. Part G, J. Aerosp. Eng.*, 2015, **229**, (9), pp. 1709–1721
[36] Chen, W.: 'Disturbance observer based control for nonlinear systems', *IEEE/ASME Trans. Mech.*, 2004, **9**, (4), pp. 706–710
[37] Khalil, H.K.: '*Nonlinear systems*' (Pearson Education Inc., New Jersey, USA, 2012, 3rd edn.)
[38] Wheeler, G., Su, C.Y., Stepanenko, Y.: 'Sliding mode controller with improved adaptation laws for the upper bounds on the norm of uncertainties', *Automatica*, 1998, **34**, (12), pp. 1657–1661